



PUBLISHED FOR SISSA BY SPRINGER

RECEIVED: October 19, 2020

ACCEPTED: December 30, 2020

PUBLISHED: February 19, 2021

Measurement of the CKM angle γ in $B^\pm \rightarrow DK^\pm$ and $B^\pm \rightarrow D\pi^\pm$ decays with $D \rightarrow K_S^0 h^+ h^-$



The LHCb collaboration

E-mail: mikkel.bjoern@physics.ox.ac.uk

ABSTRACT: A measurement of CP -violating observables is performed using the decays $B^\pm \rightarrow DK^\pm$ and $B^\pm \rightarrow D\pi^\pm$, where the D meson is reconstructed in one of the self-conjugate three-body final states $K_S^0\pi^+\pi^-$ and $K_S^0K^+K^-$ (commonly denoted $K_S^0h^+h^-$). The decays are analysed in bins of the D -decay phase space, leading to a measurement that is independent of the modelling of the D -decay amplitude. The observables are interpreted in terms of the CKM angle γ . Using a data sample corresponding to an integrated luminosity of 9 fb^{-1} collected in proton-proton collisions at centre-of mass energies of 7, 8, and 13 TeV with the LHCb experiment, γ is measured to be $(68.7_{-5.1}^{+5.2})^\circ$. The hadronic parameters r_B^{DK} , $r_B^{D\pi}$, δ_B^{DK} , and $\delta_B^{D\pi}$, which are the ratios and strong-phase differences of the suppressed and favoured B^\pm decays, are also reported.

KEYWORDS: B physics, CKM angle gamma, CP violation, Flavor physics, Hadron-Hadron scattering (experiments)

ARXIV EPRINT: [2010.08483](https://arxiv.org/abs/2010.08483)

Contents

1	Introduction	1
2	Analysis overview	2
3	LHCb detector	6
4	Selection	7
5	The DK and $D\pi$ invariant-mass spectra	9
6	CP observables	14
7	Systematic uncertainties	16
8	Interpretation	20
9	Conclusions	21
A	Correlation matrices	23
	The LHCb collaboration	30

1 Introduction

In the framework of the Standard Model, CP violation can be described by the angles and lengths of the Unitarity Triangle constructed from elements of the CKM matrix [1, 2]. The angle $\gamma \equiv \arg(-V_{ud}V_{ub}^*/V_{cd}V_{cb}^*)$ has particularly interesting features. It is the only CKM angle that can be measured in decays including only tree-level processes, and is experimentally accessible through the interference of $\bar{b} \rightarrow \bar{c}u\bar{s}$ and $\bar{b} \rightarrow \bar{u}c\bar{s}$ (and CP -conjugate) decay amplitudes. In addition, there are negligible theoretical uncertainties when interpreting the measured observables in terms of γ [3]. Hence, in the absence of unknown physics effects at tree level, a precision measurement of γ provides a Standard Model benchmark that can be compared with indirect determinations from other CKM-matrix observables more likely to be affected by physics beyond the Standard Model [4]. Such comparisons are currently limited by the precision of direct measurements of γ , which is about 5° [5, 6] dominated by LHCb results.

Decays such as $B^\pm \rightarrow DK^\pm$, where D represents a superposition of D^0 and \bar{D}^0 states, are used to observe the effects of interference between $\bar{b} \rightarrow \bar{c}u\bar{s}$ and $\bar{b} \rightarrow \bar{u}c\bar{s}$ (and CP -conjugate) decay amplitudes. The interference arises when the decay channel of the D meson is common to both D^0 and \bar{D}^0 mesons. The $B^\pm \rightarrow DK^\pm$ decay has been studied

extensively with a wide range of D -meson final states [7–11]. The exact choice of observables from each of these analyses is dependent on the method that is most appropriate for the D decay used [12–20]. The methods can be extended to a variety of different B -decay modes [8, 21–24].

This paper presents a model-independent study of the decay modes $B^\pm \rightarrow DK^\pm$ and $B^\pm \rightarrow D\pi^\pm$ where the chosen D decays are the self-conjugate decays $D \rightarrow K_S^0\pi^+\pi^-$ and $D \rightarrow K_S^0K^+K^-$ (denoted $D \rightarrow K_S^0h^+h^-$). The analysis of the $B^\pm \rightarrow DK^\pm$, $D \rightarrow K_S^0h^+h^-$ decay chain is powerful due to the rich resonance structure of the D -decay modes, as has been described in refs. [17–19]. The data used in this analysis were accumulated with the LHCb detector over the period 2011–2018 in pp collisions at energies of $\sqrt{s} = 7, 8, 13$ TeV, corresponding to a total integrated luminosity of approximately 9 fb^{-1} .

The presence of interference leads to differences in the phase-space distributions of D decays from reconstructed B^+ and B^- decays. In order to interpret any observed difference in the context of the angle γ , knowledge of the strong phase of the D^0 decay amplitude, and how it varies over phase space, is required. An attractive model-independent approach makes use of direct measurements of the strong-phase difference between D^0 and \bar{D}^0 decays, averaged over regions of the phase space [17, 25, 26]. Quantum correlated pairs of D mesons produced in decays of $\psi(3770)$ give direct access to the strong-phase differences. These have been measured by the CLEO collaboration [27], and more recently the BESIII collaboration [28–30]. Measurements using the inputs in ref. [27] have been used by the LHCb [10, 21, 31] and Belle [32, 33] collaborations. An alternate method is to use an amplitude model of the D decay to determine the strong-phase variation [34–36]. The separation of data into binned regions of the Dalitz plot leads to a loss of statistical sensitivity in comparison to using an amplitude model. However, the advantage of using the direct strong-phase measurements resides in the model-independent nature of the systematic uncertainties. Where the direct strong-phase measurements are used, there is only a systematic uncertainty associated with the finite precision of such measurements. Conversely, systematic uncertainties associated with determining a phase from an amplitude model are difficult to evaluate, as common approaches to amplitude-model building violate the optical theorem [37]. Therefore, the loss in statistical precision is compensated by reliability in the evaluation of the systematic uncertainty, which is increasingly important as the overall precision on the CKM angle γ improves. The analysis approach is laid out in section 2, while section 3 describes the LHCb detector used to collect the data sample, and section 4 summarises the selection criteria. The measurement is based on a two-step fit procedure covered in section 5, where the fit to the invariant-mass distribution is detailed, and section 6, which describes how the CP observables are determined. The systematic uncertainties are reported in section 7, and the results are interpreted to determine the value of γ in section 8. Finally, the conclusions are presented in section 9.

2 Analysis overview

The sum of the favoured and suppressed contributions to the $B^- \rightarrow DK^-$ amplitude can be written as

$$A_B(m_-^2, m_+^2) \propto A_D(m_-^2, m_+^2) + r_B^{DK} e^{i(\delta_B^{DK} - \gamma)} A_{\bar{D}}(m_-^2, m_+^2), \quad (2.1)$$

where $A_D(m_-^2, m_+^2)$ is the $D^0 \rightarrow K_S^0 h^+ h^-$ decay amplitude, and $A_{\bar{D}}(m_-^2, m_+^2)$ is the $\bar{D}^0 \rightarrow K_S^0 h^+ h^-$ decay amplitude. The hadronic parameters r_B^{DK} and δ_B^{DK} are the ratio of the magnitudes of the amplitudes of $B^- \rightarrow \bar{D}^0 K^-$ and $B^- \rightarrow D^0 K^-$ and the strong-phase difference between them, respectively. Finally, the position of the decay in the Dalitz plot is defined by m_-^2 and m_+^2 , which are the squared invariant masses of the $K_S^0 h^-$ and $K_S^0 h^+$ particle combinations, respectively. The equivalent expression for the charge-conjugated decay $B^+ \rightarrow DK^+$ is obtained by making the substitutions $\gamma \rightarrow -\gamma$ and $A_D(m_-^2, m_+^2) \leftrightarrow A_{\bar{D}}(m_-^2, m_+^2)$.

The D -decay phase space is partitioned into $2 \times \mathcal{N}$ bins labelled from $i = -\mathcal{N}$ to $i = +\mathcal{N}$ (excluding zero), symmetric around $m_-^2 = m_+^2$ such that if (m_-^2, m_+^2) is in bin i then (m_+^2, m_-^2) is in bin $-i$. The bins for which $m_-^2 > m_+^2$ are defined to have positive values of i .¹ The strong-phase difference between the D^0 - and \bar{D}^0 -decay amplitudes at a given point on the Dalitz plot is denoted as $\delta_D(m_-^2, m_+^2)$. The cosine of $\delta_D(m_-^2, m_+^2)$ weighted by the D -decay amplitude and averaged over bin i is written as c_i [17], and is given by

$$c_i \equiv \frac{\int_i dm_-^2 dm_+^2 |A_D(m_-^2, m_+^2)| |A_{\bar{D}}(m_-^2, m_+^2)| \cos [\delta_D(m_-^2, m_+^2) - \delta_{\bar{D}}(m_-^2, m_+^2)]}{\sqrt{\int_i dm_-^2 dm_+^2 |A_D(m_-^2, m_+^2)|^2 \int_i dm_-^2 dm_+^2 |A_{\bar{D}}(m_-^2, m_+^2)|^2}}, \quad (2.2)$$

where the integrals are evaluated over bin i . An analogous expression can be written for s_i , which is the sine of the strong-phase difference weighted by the decay amplitude and averaged over the bin phase space.

The expected yield of B^- decays in bin i is found by integrating the square of the amplitude given in eq. (2.1) over the region of phase space defined by the i th bin. The effects of charm mixing and CP violation are ignored, as is the presence of CP violation and matter regeneration in the neutral K^0 decays. These effects are expected to have a small impact [38, 39] on the distribution of events on the Dalitz plot. Selection requirements and reconstruction effects lead to a non-uniform efficiency over phase space, denoted by $\eta(m_-^2, m_+^2)$. At LHCb the typical efficiency variation over phase space for a $D \rightarrow K_S^0 h^+ h^-$ decay from a region of high efficiency to low efficiency is approximately 60% [21]. The fractional yield of pure D^0 decays in bin i in the presence of this efficiency profile is denoted F_i , given by

$$F_i = \frac{\int_i dm_-^2 dm_+^2 |A_D(m_-^2, m_+^2)|^2 \eta(m_-^2, m_+^2)}{\sum_j \int_j dm_-^2 dm_+^2 |A_D(m_-^2, m_+^2)|^2 \eta(m_-^2, m_+^2)}, \quad (2.3)$$

where the sum in the denominator is over all Dalitz plot bins, indexed by j . Neglecting CP violation in these charm decays, the charge-conjugate amplitudes satisfy the relation $A_{\bar{D}}(m_-^2, m_+^2) = A_D(m_+^2, m_-^2)$, and therefore $F_i = \bar{F}_{-i}$, where \bar{F}_i is the fractional yield of \bar{D}^0 decays to bin i . The physics parameters of interest, r_B^{DK} , δ_B^{DK} , and γ , are translated into four CP -violating observables [40] that are measured in this analysis and are the real and imaginary parts of the ratio of the suppressed and favoured B decay amplitudes,

$$x_{\pm}^{DK} \equiv r_B^{DK} \cos(\delta_B^{DK} \pm \gamma) \quad \text{and} \quad y_{\pm}^{DK} \equiv r_B^{DK} \sin(\delta_B^{DK} \pm \gamma). \quad (2.4)$$

¹For historical reasons, this convention defines positive bins in the opposite manner to that used to determine the charm strong-phase differences in $D \rightarrow K_S^0 h^+ h^-$ decays.

Using the relations $c_i = c_{-i}$ and $s_i = -s_{-i}$ the B^+ (B^-) yields, N^+ (N^-), in bin i and $-i$ are given by

$$\begin{aligned}
 N_{+i}^+ &= h_{B^+} \left[F_{-i} + \left((x_+^{DK})^2 + (y_+^{DK})^2 \right) F_{+i} + 2\sqrt{F_i F_{-i}} \left(x_+^{DK} c_{+i} - y_+^{DK} s_{+i} \right) \right], \\
 N_{-i}^+ &= h_{B^+} \left[F_{+i} + \left((x_+^{DK})^2 + (y_+^{DK})^2 \right) F_{-i} + 2\sqrt{F_i F_{-i}} \left(x_+^{DK} c_{+i} + y_+^{DK} s_{+i} \right) \right], \\
 N_{+i}^- &= h_{B^-} \left[F_{+i} + \left((x_-^{DK})^2 + (y_-^{DK})^2 \right) F_{-i} + 2\sqrt{F_i F_{-i}} \left(x_-^{DK} c_{+i} + y_-^{DK} s_{+i} \right) \right], \\
 N_{-i}^- &= h_{B^-} \left[F_{-i} + \left((x_-^{DK})^2 + (y_-^{DK})^2 \right) F_{+i} + 2\sqrt{F_i F_{-i}} \left(x_-^{DK} c_{+i} - y_-^{DK} s_{+i} \right) \right],
 \end{aligned} \tag{2.5}$$

where h_{B^+} and h_{B^-} are normalisation constants. The value of r_B^{DK} is allowed to be different for each charge and is constructed from either $(r_B^{DK})^2 = (x_+^{DK})^2 + (y_+^{DK})^2$ or $(r_B^{DK})^2 = (x_-^{DK})^2 + (y_-^{DK})^2$. A single value of r_B^{DK} is determined when the CP observables are subsequently interpreted to determine the physics parameters of interest. The normalisation constants can be written as a function of γ , analogous to the global asymmetries studied in decays where the D meson decays to a CP eigenstate [8]. However, not only is this global asymmetry expected to be small since the CP -even content of the $D \rightarrow K_S^0 \pi^+ \pi^-$ and $D \rightarrow K_S^0 K^+ K^-$ decay modes is close to 0.5, it is also expected to be heavily biased due to the effects of K_S^0 CP violation [39] on total yields. Therefore the global asymmetry is ignored and the loss of information is minimal. An advantage of this approach is that the normalisation constants h_{B^+} and h_{B^-} are independent of each other, and will implicitly contain the effects of the production asymmetry of B^\pm mesons in pp collisions and the detection asymmetries of the charged kaon from the B decay. This leads to a CP -violation measurement that is free of systematic uncertainties associated to these effects.

The system of equations provides $4\mathcal{N}$ observables and $4+2\mathcal{N}$ unknowns, assuming that the available measurements of c_i and s_i are used. This is solvable for $\mathcal{N} \geq 2$, but in practice the simultaneous fit of the F_i , x_\pm^{DK} , and y_\pm^{DK} parameters leads to large uncertainties on the CP observables, and hence some external knowledge of the F_i parameters is desirable. The F_i parameters could be computed from simulation and an amplitude model, but the systematic uncertainties associated with the LHCb simulation would be significant. Recent analyses [10, 31] have used the semileptonic decay $B \rightarrow D^* \mu \nu$, where the flavour-tagged yields of D^0 mesons are corrected for the differences in selection between the semileptonic channel and the signal mode. However, with the increased signal yields, the uncertainty due to this necessary correction will be approximately half the statistical uncertainty on the measurement presented in this paper, and therefore a different method is adopted.

The $B^\pm \rightarrow D\pi^\pm$ decay mode is expected to have F_i parameters that are the same as those for $B^\pm \rightarrow DK^\pm$ if a similar selection is applied due to the common topology and the ability to use same signatures in the detector to select the candidates. The $B^\pm \rightarrow D\pi^\pm$ decay is expected to exhibit CP violation through the interference of $\bar{b} \rightarrow \bar{c}u\bar{d}$ and $\bar{b} \rightarrow \bar{u}c\bar{d}$ transitions, analogous to the $B^\pm \rightarrow DK^\pm$ decay but suppressed by one order of magnitude [41]. Further effects from K_S^0 CP violation and matter regeneration have been recently shown to have only a small impact on the *distribution* over the Dalitz plot [39], in contrast to

their impact on the global asymmetry. Therefore the $B^\pm \rightarrow D\pi^\pm$ channel can be used to determine the F_i parameters if the small level of CP violation in the B^\pm decay is accounted for.

Pseudoexperiments are performed in which the two B -decay modes are fit together assuming common F_i parameters. Independent x_\pm and y_\pm observables are required for the two B decay modes due to different values of the hadronic parameters, r_B and δ_B . The value of r_B in $B^\pm \rightarrow DK^\pm$ is approximately 0.1, and it is expected that it will be a factor 20 smaller in $B^\pm \rightarrow D\pi^\pm$ decays [41]. The yields of $B^\pm \rightarrow D\pi^\pm$ are described by a set of equations analogous to eq. (2.5), with the substitutions $x_\pm^{DK} \rightarrow x_\pm^{D\pi}$ and $y_\pm^{DK} \rightarrow y_\pm^{D\pi}$. An analysis that simultaneously measures the F_i , x_\pm^{DK} , y_\pm^{DK} , $x_\pm^{D\pi}$, and $y_\pm^{D\pi}$ parameters is found to be stable only if $r_B^{D\pi} > 0.03$. At the expected value $r_B^{D\pi} = 0.005$ the fit is unstable due to high correlations between the F_i and $x_\pm^{D\pi}$ and $y_\pm^{D\pi}$. Therefore an alternate parameterisation [42, 43] is introduced, which utilises the fact that γ is a common parameter, and that the CP violation in $B^\pm \rightarrow D\pi^\pm$ decays can therefore be described by the addition of a single complex variable

$$\xi^{D\pi} = \left(\frac{r_B^{D\pi}}{r_B^{DK}} \right) \exp(i\delta_B^{D\pi} - i\delta_B^{DK}), \quad (2.6)$$

and in terms of $x_\xi^{D\pi} \equiv \text{Re}(\xi^{D\pi})$ and $y_\xi^{D\pi} \equiv \text{Im}(\xi^{D\pi})$, the $(x_\pm^{D\pi}, y_\pm^{D\pi})$ parameters are given by

$$x_\pm^{D\pi} = x_\xi^{D\pi} x_\pm^{DK} - y_\xi^{D\pi} y_\pm^{DK}, \quad y_\pm^{D\pi} = x_\xi^{D\pi} y_\pm^{DK} + y_\xi^{D\pi} x_\pm^{DK}. \quad (2.7)$$

With this parameterisation, the simultaneous fit to x_\pm^{DK} , y_\pm^{DK} , $x_\xi^{D\pi}$, $y_\xi^{D\pi}$ (the CP observables) and F_i parameters is stable for all values of $r_B^{D\pi}$. The simultaneous fit of $B^\pm \rightarrow D\pi^\pm$ and $B^\pm \rightarrow DK^\pm$ candidates has two advantages. Firstly, the extraction of F_i in this manner is expected to have negligible associated systematic uncertainty, and reduces significantly the reliance on simulation. Secondly, the CP -violating observables in $B^\pm \rightarrow D\pi^\pm$ using other D -decay modes [8, 9] are not routinely included in the γ combination of all results because they allow for two solutions of $(r_B^{D\pi}, \delta_B^{D\pi})$, which makes the statistical interpretation of the full $B^\pm \rightarrow Dh^\pm$ combination problematic [44]. The measurement in the $B^\pm \rightarrow D\pi^\pm$, $D \rightarrow K_S^0 h^+ h^-$ decays has the potential to resolve this redundancy, and allow for a more straightforward inclusion of all $B^\pm \rightarrow D\pi^\pm$ results in the combination. A small disadvantage is that the measurement of γ will incorporate information from both $B^\pm \rightarrow DK^\pm$ and $B^\pm \rightarrow D\pi^\pm$ decay modes and the contribution of each cannot be disentangled. However, since the size of contribution from the $B^\pm \rightarrow D\pi^\pm$ decay to the precision is expected to be negligible in comparison to that from the $B^\pm \rightarrow DK^\pm$ decay, this is considered an acceptable compromise.

The measurements of c_i and s_i are available in four different 2×8 binning schemes for the $D \rightarrow K_S^0 \pi^+ \pi^-$ decay. This analysis uses the scheme called the optimal binning, where the bins have been chosen to optimise the statistical sensitivity to γ , as described in ref. [27]. The optimisation was performed assuming a strong-phase difference distribution as predicted by the BaBar model presented in ref. [45]. For the $K_S^0 K^+ K^-$ final state, three choices of binning schemes are available, containing 2×2 , 2×3 , and 2×4 bins. The guiding model used to determine the bin boundaries is taken from the BaBar study described in ref. [46].

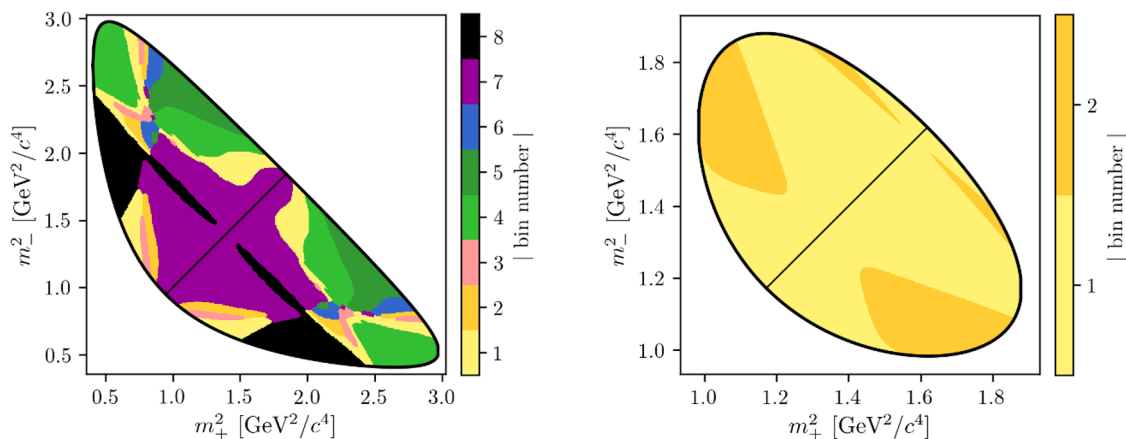


Figure 1. Binning schemes for (left) $D \rightarrow K_S^0 \pi^+ \pi^-$ decays and (right) $D \rightarrow K_S^0 K^+ K^-$ decays. The diagonal line separates the positive and negative bins, where the positive bins are in the region in which $m_-^2 > m_+^2$ is satisfied.

The $D \rightarrow K_S^0 K^+ K^-$ decay mode is dominated by the intermediate $K_S^0 \phi$ and $K_S^0 a(980)$ states which are CP -odd and CP -even, respectively, and the narrow $K_S^0 \phi$ resonance is encapsulated within the second bin of the 2×2 scheme. Therefore, most of the sensitivity is encompassed by this scheme, and the additional small gains from the more detailed schemes are offset by low yields and fit instabilities that arise when these bins are used. Therefore, the 2×2 bin is used for the analysis of the $D \rightarrow K_S^0 K^+ K^-$ decay mode. The measurements of c_i and s_i are not biased by the use of a specific amplitude model in defining the bin boundaries. The choice of the model only affects this analysis to the extent that a poor model description of the underlying decay would result in a reduced statistical sensitivity of the γ measurement. The binning choices for the two decay modes are shown in figure 1.

Measurements of the c_i and s_i parameters in the optimal binning scheme for the $D \rightarrow K_S^0 \pi^+ \pi^-$ decay and in the 2×2 binning scheme for the $D \rightarrow K_S^0 K^+ K^-$ decay are available from both the CLEO and BESIII collaborations. A combination of results from both collaborations is presented in ref. [29] and ref. [30] for the $D \rightarrow K_S^0 \pi^+ \pi^-$ and $D \rightarrow K_S^0 K^+ K^-$ decays, respectively. The combinations are used within this analysis.

3 LHCb detector

The LHCb detector [47, 48] is a single-arm forward spectrometer covering the pseudorapidity range $2 < \eta < 5$, designed for the study of particles containing b or c quarks. The detector includes a high-precision tracking system consisting of a silicon-strip vertex detector surrounding the pp interaction region, a large-area silicon-strip detector located upstream of a dipole magnet with a bending power of about 4 Tm, and three stations of silicon-strip detectors and straw drift tubes placed downstream of the magnet. The tracking system provides a measurement of the momentum, p , of charged particles with a relative uncertainty that varies from 0.5% at low momentum to 1.0% at 200 GeV/c. The minimum

distance of a track to a primary vertex (PV), the impact parameter (IP), is measured with a resolution of $(15 + 29/p_T) \mu\text{m}$, where p_T is the component of the momentum transverse to the beam, in GeV/c . Different types of charged hadrons are distinguished using information from two ring-imaging Cherenkov detectors. Photons, electrons and hadrons are identified by a calorimeter system consisting of scintillating-pad and preshower detectors, an electromagnetic and a hadronic calorimeter. Muons are identified by a system composed of alternating layers of iron and multiwire proportional chambers. The online event selection is performed by a trigger, which consists of a hardware stage, based on information from the calorimeter and muon systems, followed by a software stage, which applies a full event reconstruction. The events that are selected for the analysis either have final-state tracks of the signal decay that are subsequently associated with an energy deposit in the calorimeter system that satisfies the hardware stage trigger, or are selected because one of the other particles in the event, not reconstructed as part of the signal candidate, fulfills any hardware stage trigger requirement. At the software stage, it is required that at least one particle should have high p_T and high χ_{IP}^2 , where χ_{IP}^2 is defined as the difference in the primary vertex fit χ^2 with and without the inclusion of that particle. A multivariate algorithm [49] is used to identify secondary vertices consistent with being a two-, three-, or four-track b -hadron decay. The PVs are fitted with and without the tracks of the decay products of the B candidate, and the PV that gives the smallest χ_{IP}^2 is associated with the B candidate.

Simulation is required to model the invariant-mass distributions of the signal and background contributions and determine the selection efficiencies of the background relative to the signal decay modes. It is also used to provide an approximation for the efficiency variations over the phase space of the D decay for systematic studies. In the simulation, pp collisions are generated using PYTHIA [50, 51] with a specific LHCb configuration [52]. Decays of unstable particles are described by EVTGEN [53], in which final-state radiation is generated using PHOTOS [54]. The decays $D \rightarrow K_S^0 \pi^+ \pi^-$ and $D \rightarrow K_S^0 K^+ K^-$ are generated uniformly over phase space. The interaction of the generated particles with the detector, and its response, are implemented using the GEANT4 toolkit [55, 56] as described in ref. [57]. With the exception of the signal decay, the simulated event is reused multiple times [58]. Some subdominant backgrounds are generated with a fast simulation [59] that can mimic the geometric acceptance and tracking efficiency of the LHCb detector as well as the dynamics of the decay.

4 Selection

The selection closely follows that of ref. [10]. Decays of $K_S^0 \rightarrow \pi^+ \pi^-$ are reconstructed in two different ways: the first involving K_S^0 mesons that decay early enough for the pions to be reconstructed in the vertex detector; and the second containing K_S^0 that decay later such that track segments of the pions cannot be formed in the vertex detector. The first and second types of reconstructed K_S^0 decays are referred to as *long* and *downstream* candidates, respectively. The *long* candidates have the best mass, momentum and vertex resolution, but approximately two-thirds of the signal candidates belong to the *downstream* category.

The D meson candidates are built by combining a K_S^0 candidate with two tracks assigned either the pion or kaon hypothesis. A B candidate is then formed by combining the D meson candidate with a further track. At each stage of combination, selection requirements are placed to ensure good quality vertices, and K_S^0 and D candidate invariant-masses are required to be close to their nominal mass [60]. Mutually exclusive particle identification (PID) requirements are placed on the companion track from the B decay to separate $B^\pm \rightarrow DK^\pm$ and $B^\pm \rightarrow D\pi^\pm$ candidates, where the companion refers to the final state π^\pm or K^\pm meson produced in the $B^\pm \rightarrow Dh^\pm$ decay. PID requirements are also placed on the charged decay products of the D meson to reduce combinatorial background. A series of selection requirements are placed on the candidates to remove background from other B meson decays. A background from $B^\pm \rightarrow Dh^\pm$ decays where the D meson decays to either $\pi^+\pi^-\pi^+\pi^-$ or $K^+K^-\pi^+\pi^-$ is rejected by requiring that the *long* K_S^0 candidates decay a significant distance from the D vertex. Similarly, the D meson is required to have travelled a significant distance from the B vertex to suppress B decays with the same final state, but where there is no intermediate D meson decay. Semileptonic decays of the type $D^0 \rightarrow K^{*-}l^+\nu$, where charge-conjugate decays are implied, can be reconstructed as $D \rightarrow K_S^0 h^+ h^-$ with expected contamination rates of the order of a percent. To suppress electron to pion misidentification, a veto is placed on the pion from the D decay that has the opposite charge with respect to the companion particle, if the PID response suggests it is an electron. To suppress the similar muonic background, it is required that the charged track from the D decay has no corresponding activity in the muon detector. This veto also suppresses signal decays where the pion or kaon meson decays before reaching the muon detector. Therefore, it is applied on both charged tracks from the D decay, as these events have a worse resolution on the Dalitz plot, which is undesirable. Finally, the same requirement is placed on the companion track to suppress $B \rightarrow D\mu\nu$ decays.

The large remaining combinatorial background is suppressed through the use of a boosted decision tree (BDT) [61, 62] multivariate classifier. The BDT is trained on simulated signal events. The background training sample is obtained from the far upper sideband of the $m(Dh^\pm)$ mass distribution between 5800-7000 MeV/ c^2 , in order to provide a sample independent from the data which will be used in the fit to determine the CP observables. A separate BDT is trained for B decays containing *long* or *downstream* K_S^0 candidates. The input variables given to each BDT include momenta of the B , D , and companion particles, the absolute and relative positions of decay vertices, as well as parameters that quantify the fit quality in the reconstruction; the parameter set is identical to the one used in the previous LHCb measurement and listed in detail in ref. [10]. The BDT has been proven not to bias the $m(Dh^\pm)$ distribution. A series of pseudoexperiments are run to find the threshold values for the two BDTs which provide the best sensitivity to γ . This requirement rejects approximately 98% of the combinatorial background that survives all other selection requirements, while having an efficiency of approximately 93% in simulated $B^\pm \rightarrow DK^\pm$ decays. The selection applied to $B^\pm \rightarrow DK^\pm$ and $B^\pm \rightarrow D\pi^\pm$ candidates is identical between the two decay modes with the exception of the PID requirement on the companion track.

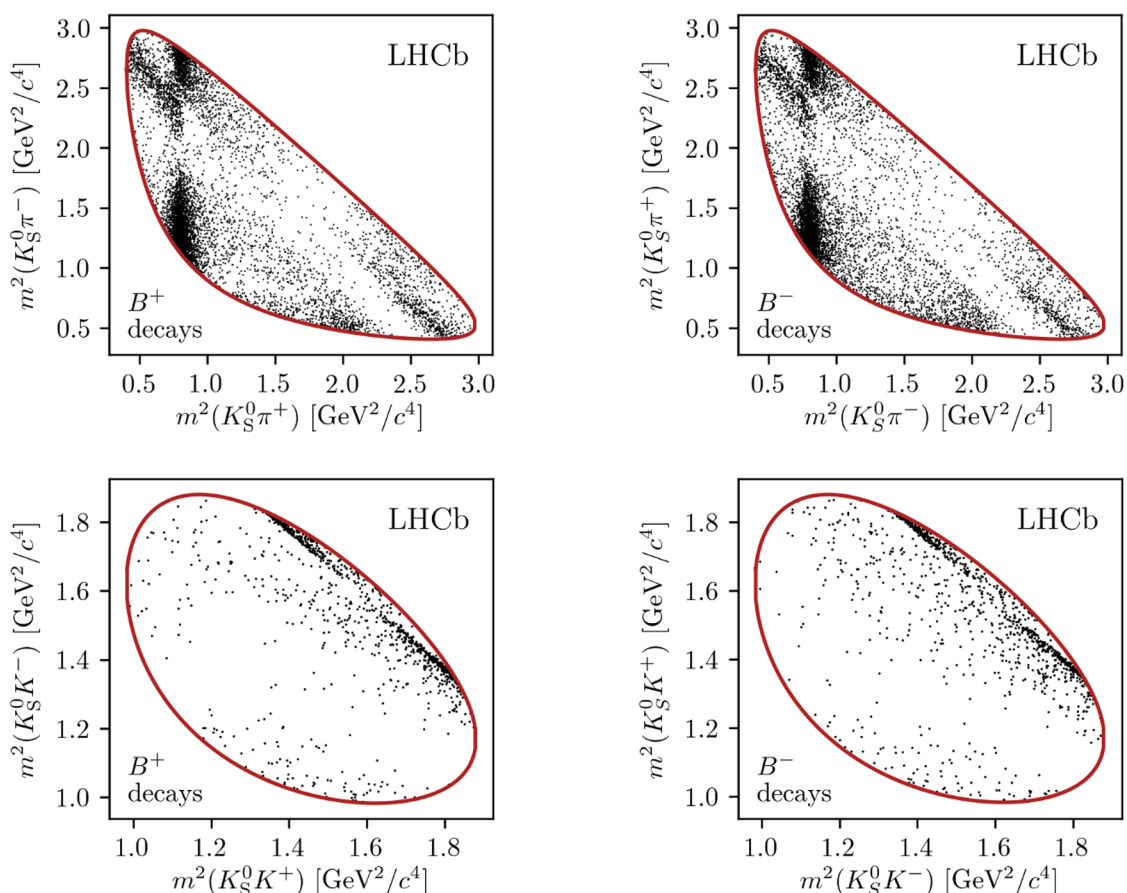


Figure 2. Dalitz plot for D decays of (left) $B^+ \rightarrow DK^+$ and (right) $B^- \rightarrow DK^-$ candidates in the signal region, in the (top) $D \rightarrow K_S^0 \pi^+ \pi^-$ and (bottom) $D \rightarrow K_S^0 K^+ K^-$ channels. The horizontal and vertical axes are interchanged between the B^+ and B^- decay plots to aid visualisation of the CP asymmetries between the two distributions.

A signal region is defined as within $30 \text{ MeV}/c^2$ of the B -meson mass [60]. The phase-space distributions for candidates in this range are shown in the Dalitz plots of figure 2 for $B^\pm \rightarrow DK^\pm$ candidates. The data are split by the final state of the D decay and by the charge of the B meson. Small differences between the phase-space distributions in $B^+ \rightarrow DK^+$ and $B^- \rightarrow DK^-$ decays are visible in the $K_S^0 \pi^+ \pi^-$ final state.

5 The DK and $D\pi$ invariant-mass spectra

The analysis uses a two-stage strategy to determine the CP observables. First, an extended maximum-likelihood fit to the invariant-mass spectrum of all selected B^\pm candidates in the mass range 5080 to $5800 \text{ MeV}/c^2$ is performed, with no partition of the D phase space. This fit is referred to as the *global* fit. The global fit is used to determine the signal and background component parameterisations, which are subsequently used in a second stage

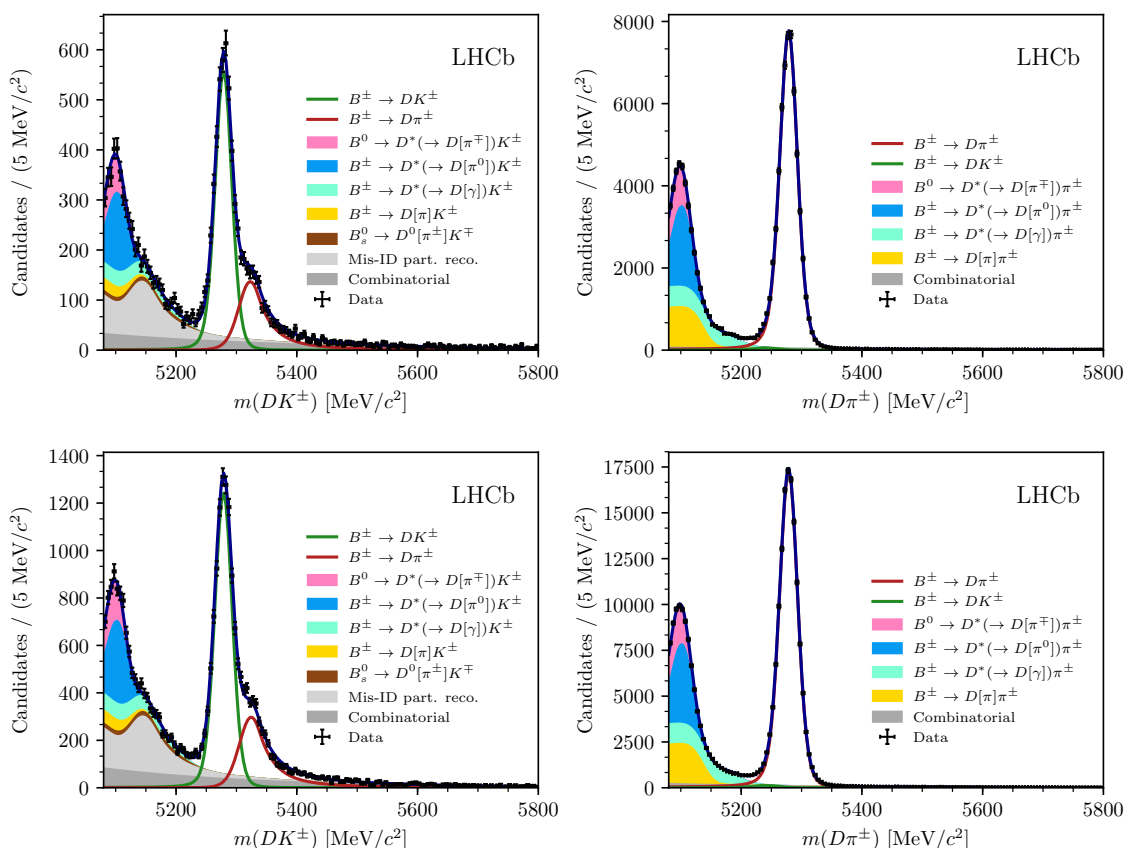


Figure 3. Invariant mass distributions for the (left) $B^\pm \rightarrow DK^\pm$ channel and (right) $B^\pm \rightarrow D\pi^\pm$ channel with $D \rightarrow K_S^0\pi^+\pi^-$. The top (bottom) plots show data where the K_S^0 candidate is *long* (*downstream*). Square brackets in the legend denote a particle that has not been reconstructed.

where the data are split by B charge and partitioned into the Dalitz plot bins to determine the CP observables.

The invariant mass distributions of the selected B^\pm candidates are shown for $D \rightarrow K_S^0\pi^+\pi^-$ and $D \rightarrow K_S^0K^+K^-$ candidates in figures 3 and 4, respectively, together with the results of the global fit superimposed. The invariant mass is kinematically constrained through a fit imposed on the full B^\pm decay chain [63]. The D and K_S^0 candidates are constrained to their known masses [60] and the B^\pm candidate momentum vector is required to point towards the associated PV. The data sample is split into 8 categories depending on the reconstructed B decay, D decay mode, and K_S^0 category, since the latter exhibits slightly different mass resolutions. The fit is performed simultaneously for all categories in order to allow parameters to be shared.

The peaks centered around $5280 \text{ MeV}/c^2$ correspond to the signal $B^\pm \rightarrow DK^\pm$ and $B^\pm \rightarrow D\pi^\pm$ candidates. The parameterisation for the signal invariant-mass shape is determined from simulation; the invariant-mass distribution is modelled with a sum of the probability density function (PDF) for a Gaussian distribution, $f_G(m|m_B, \sigma)$, and a modified Gaussian PDF that is used to account for the radiative tail and the wider resolution

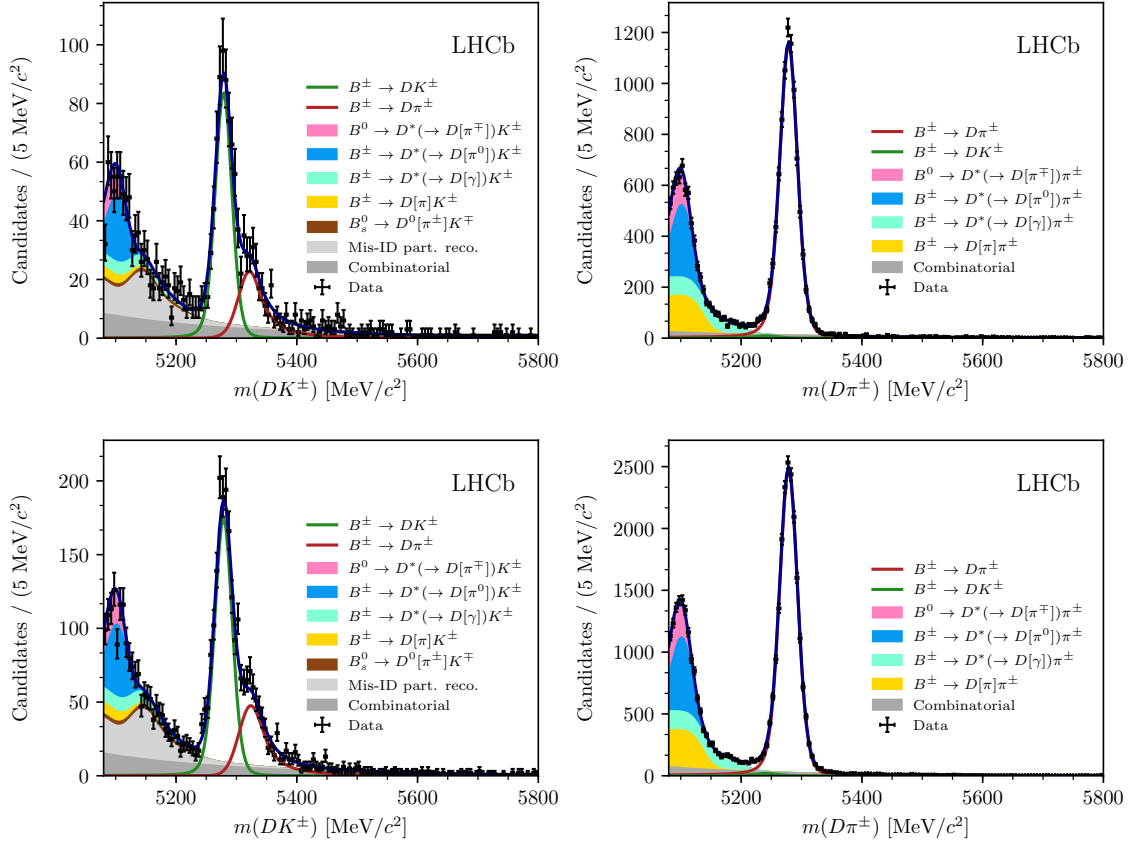


Figure 4. Invariant mass distributions for the (left) $B^\pm \rightarrow DK^\pm$ channel and (right) $B^\pm \rightarrow D\pi^\pm$ channel with $D \rightarrow K_S^0 K^+ K^-$. The top (bottom) plots show data where the K_S^0 candidate is *long* (*downstream*). Square brackets in the legend denote a particle that has not been reconstructed.

of signal events that are poorly reconstructed. The modified Gaussian has the form

$$f_{\text{MG}}(m|m_B, \sigma, \alpha_L, \alpha_R, \beta) \propto \begin{cases} \exp\left[\frac{-\Delta m^2(1+\beta\Delta m^2)}{2\sigma^2+\alpha_L\Delta m^2}\right], & \Delta m = m - m_B < 0 \\ \exp\left[\frac{-\Delta m^2(1+\beta\Delta m^2)}{2\sigma^2+\alpha_R\Delta m^2}\right], & \Delta m = m - m_B > 0, \end{cases} \quad (5.1)$$

which is Gaussian when $\Delta m^2 \ll \sigma^2/\alpha_{L/R}$ or $\Delta m^2 \gg \beta^{-1}$ (with widths of σ and $\sqrt{\alpha_{L/R}/\beta}$, respectively), with an exponential-like transition that is able to model the effect of the experimental resolution of LHCb. Thus, the signal PDF has the form

$$f_{\text{signal}}(m|m_B, \sigma, \alpha_L, \alpha_R, \beta, k) = k \cdot f_{\text{MG}}(m|m_B, \sigma, \alpha_L, \alpha_R, \beta) + (1 - k) \cdot f_{\text{G}}(m|m_B, \sigma) \quad (5.2)$$

The values of the tail parameters ($\alpha_L, \alpha_R, \beta$) and k are fixed from simulation and are common for the two D decays (which is possible due to the applied kinematic constraints) but different for each B decay and type of K_S^0 candidate. The signal mass, m_B , is determined in data and is the same for all categories. The width, σ , of the signal PDF is determined by

the data and allowed to be different for each B decay and type of K_S^0 candidate. The width is narrower in $B^\pm \rightarrow DK^\pm$ decays compared to $B^\pm \rightarrow D\pi^\pm$ decays due to the smaller free energy in the decay. The width is approximately 3% narrower in decays with *long* K_S^0 candidates. The signal yield is determined in each of the categories where the candidates are reconstructed as $B^\pm \rightarrow D\pi^\pm$. The signal yield in the corresponding category where the candidates are reconstructed as $B^\pm \rightarrow DK^\pm$ is determined by multiplying the $B^\pm \rightarrow D\pi^\pm$ yield by the parameters $\mathcal{B} \times \epsilon$. The parameter \mathcal{B} corresponds to the ratio of the branching fractions for $B^\pm \rightarrow DK^\pm$ and $B^\pm \rightarrow D\pi^\pm$ decays, while the correction factor, ϵ , takes into account the ratio of PID and selection efficiencies, and is determined for each pair of $B^\pm \rightarrow DK^\pm$ and $B^\pm \rightarrow D\pi^\pm$ categories and fixed in the fit. The parameter \mathcal{B} is shared across all categories and is found to be consistent with ref. [60].

To the right of the $B^\pm \rightarrow DK^\pm$ peak there is a visible contribution from $B^\pm \rightarrow D\pi^\pm$ decays that are reconstructed as $B^\pm \rightarrow DK^\pm$ decays. The corresponding contribution in the $B^\pm \rightarrow D\pi^\pm$ category is minimal due to the smaller branching fraction of $B^\pm \rightarrow DK^\pm$, but is accounted for in the fit. The rates of these cross-feed backgrounds are fixed from PID efficiencies determined in calibration data, which is reweighted to match the momentum and pseudorapidity distributions of the companion track of the signal. A data-driven approach is used to determine the PDF of $B^\pm \rightarrow D\pi^\pm$ decays that are reconstructed as $B^\pm \rightarrow DK^\pm$ candidates, by using $B^\pm \rightarrow D\pi^\pm$ decays and recalculating the invariant mass when the Kaon hypothesis is applied to the companion particle. Full details of the procedure are described in ref. [10]. The same procedure is implemented to determine the PDF of $B^\pm \rightarrow DK^\pm$ decays reconstructed as $B^\pm \rightarrow D\pi^\pm$ candidates.

The background observed at invariant masses smaller than the signal peak are candidates that originate from other B -meson decays where not all decay products have been reconstructed. Due to the selected invariant-mass range it is only necessary to consider B meson decays where a single photon or pion has not been reconstructed. This background type is split into three sources; the first where the candidate originates from a B^\pm or B^0 meson, referred to as partially reconstructed background, the second where the candidate originates from a B_s^0 meson, and the third where the candidate originates from a B^\pm or B^0 and furthermore one of the reconstructed tracks is assigned the kaon hypothesis, when the true particle is a pion. The latter type of background appears in the $B^\pm \rightarrow DK^\pm$ candidates and is referred to as misidentified partially reconstructed background. The corresponding type of background is not modelled in the $B^\pm \rightarrow D\pi^\pm$ candidates, since it is suppressed due to the branching fractions involved and the majority is removed by the lower invariant-mass requirement.

There are contributions from $B^0 \rightarrow D^{*\pm}h^\mp$ and $B^\pm \rightarrow D^{*0}h^\pm$ decays in all categories, where the pion or the photon originating from the D^* meson is not reconstructed. The invariant-mass distributions of these decays depend on the spin and mass of the missing particle as described in ref. [24]. The parameters of these shapes are determined from simulation, with the exception of a free parameter in the fit to characterise the resolution. The decays $B^{\pm,0} \rightarrow D\pi^\pm\pi^{0,\mp}$ contribute to the $B^\pm \rightarrow D\pi^\pm$ candidates where one of the pions from the B decay is not reconstructed. The shape of this background is determined from simulated $B^\pm \rightarrow D\rho^\pm$ and $B^0 \rightarrow D\rho^0$ decays. The decays $B^\pm \rightarrow DK^\pm\pi^0$

and $B^0 \rightarrow DK^+\pi^-$ contribute to the $B^\pm \rightarrow DK^\pm$ candidates where the pion is not reconstructed. The invariant-mass distribution for these events is based on the amplitude model of $B^0 \rightarrow DK^+\pi^-$ decays [64]. The model is used to generate four-vectors of the decay products, which are smeared to account for the LHCb detector resolution. The invariant mass is then calculated omitting the particle that is not reconstructed, and this distribution is subsequently fit to determine the fixed distribution for the fit. The same shape is used for the $B^\pm \rightarrow DK^\pm\pi^0$ decay as the corresponding amplitude model is not available. Finally, the $B^\pm \rightarrow DK^\pm$ candidates also have a contribution from $B_s^0 \rightarrow \bar{D}^0\pi^+K^-$ decays where the pion is not reconstructed. The shape of this contribution is determined in a similar manner to that of $B^0 \rightarrow DK^+\pi^-$ decays using the $B_s^0 \rightarrow \bar{D}^0\pi^+K^-$ amplitude model determined in ref. [65].

The yield of the partially reconstructed background is a free parameter in each $B^\pm \rightarrow D\pi^\pm$ sample and related to the yield in the corresponding $B^\pm \rightarrow DK^\pm$ sample via the free parameter $\mathcal{B}_{\mathcal{L}}$ and correction factors from PID and selection efficiencies. Analogously to the signal-yield parameterisation, $\mathcal{B}_{\mathcal{L}}$ is a single parameter, common to all categories, but in this case has no direct physical meaning. The relative yield of $B^\pm \rightarrow D^*(\rightarrow D[\gamma])\pi^\pm$ and $B^0 \rightarrow D^*(\rightarrow D[\pi^\mp])\pi^\pm$ decays, where the particle within the square brackets is the one not reconstructed, are fixed from branching fractions [60], and selection efficiencies determined from simulation. The fractional yields of $B^\pm \rightarrow D^{*0}(\rightarrow D[\gamma])\pi^\pm$, and $B^{\pm,0} \rightarrow D[\pi^{0,\mp}]\pi^\pm$ decays are determined in the fit and are constrained to be the same for each $B^\pm \rightarrow D\pi^\pm$ sample. Due to the lower yields in the $B^\pm \rightarrow DK^\pm$ category and presence of additional backgrounds, the relative fractions of the various B^\pm and B^0 components are all fixed using information from branching fractions [60] and selection efficiencies from simulation. The yield of the $B_s^0 \rightarrow \bar{D}^0\pi^+K^-$ decays is fixed relative to the yield of $B^\pm \rightarrow D\pi^\pm$ decays in the corresponding category using branching fractions [60], the fragmentation fraction [66], and relative selection efficiencies. Hence in total there are six free parameters to determine the partially reconstructed background yields. Four of these measure the yield in each $B^\pm \rightarrow D\pi^\pm$ sample and a further single parameter determines the yield in the corresponding $B^\pm \rightarrow DK^\pm$ sample. A final floating parameter determines the relative yield between two of the background components.

The shapes for the misidentified partially reconstructed backgrounds are determined from simulation, weighted by the PID efficiencies from calibration data. The yield of these backgrounds are determined from the partially reconstructed yields in the $B^\pm \rightarrow D\pi^\pm$ candidates, and the relative selection efficiencies, which include the PID efficiencies from calibration data and the selection efficiency due to requiring the reconstructed invariant mass to be above 5080 MeV/c². The final component of background is combinatorial which is parameterised by an exponential function. The yield and slope of this background in each category are free parameters. The yields of the different signals and background types are integrated in the signal region 5249–5309 MeV/c² and reported in table 1. The $B^\pm \rightarrow DK^\pm$ yields in categories of different D decay and type of K_S^0 candidate have uncertainties that are smaller than their Poisson uncertainty since they are determined using the value of \mathcal{B} , which is measured from all $B^\pm \rightarrow DK^\pm$ candidates.

Reconstructed as:		$B^\pm \rightarrow DK^\pm$		$B^\pm \rightarrow D\pi^\pm$	
D decay	Component	<i>long</i>	<i>downstream</i>	<i>long</i>	<i>downstream</i>
$D \rightarrow K_S^0 \pi^+ \pi^-$	$B^\pm \rightarrow DK^\pm$	3798 ± 41	8735 ± 89	182 ± 3	433 ± 8
	$B^\pm \rightarrow D\pi^\pm$	342 ± 3	691 ± 5	55096 ± 240	124786 ± 368
	Part. reco. background	114 ± 3	246 ± 6	36 ± 7	81 ± 12
	Combinatorial	206 ± 36	458 ± 60	392 ± 66	1142 ± 127
$D \rightarrow K_S^0 K^+ K^-$	$B^\pm \rightarrow DK^\pm$	576 ± 8	1203 ± 15	29 ± 1	61 ± 1
	$B^\pm \rightarrow D\pi^\pm$	56 ± 1	104 ± 2	8196 ± 92	17863 ± 137
	Part. reco background	17 ± 2	34 ± 2	5 ± 3	11 ± 5
	Combinatorial	44 ± 13	75 ± 20	127 ± 32	288 ± 52

Table 1. The signal and background yields in the region $m_B \in [5249, 5309]$ MeV/ c^2 as obtained in the fit. For the $B^\pm \rightarrow DK^\pm$ candidates, the yield of the partially reconstructed background includes the contributions from B_S^0 decays and misidentified partially reconstructed backgrounds.

6 CP observables

To determine the CP observables the data are divided into 16 categories (B decay, B charge, D decay, type of K_S^0 candidate) and then further split into each Dalitz plot bin. A simultaneous fit to the invariant-mass distribution is performed in all categories and Dalitz plot bins. The mass shape parameters are all fixed from the global mass fit. The lower limit of the invariant mass is increased to 5150 MeV/ c^2 to remove a large fraction of the partially reconstructed background. The signal yield in each bin is parameterised using eq. (2.5) or the analogous set of expressions for $B^\pm \rightarrow D\pi^\pm$. These equations are normalised such that the parameters h_{B^\pm} represent the total observed signal yield in each category, and these are measured independently. The yield of misidentified $B^\pm \rightarrow D\pi^\pm$ ($B^\pm \rightarrow DK^\pm$) decays in each $B^\pm \rightarrow DK^\pm$ ($B^\pm \rightarrow D\pi^\pm$) sample is determined by the PID efficiencies and the signal yield in the corresponding $B^\pm \rightarrow D\pi^\pm$ ($B^\pm \rightarrow DK^\pm$) sample.

The parameters x_\pm^{DK} , y_\pm^{DK} , $x_\xi^{D\pi}$, and $y_\xi^{D\pi}$ are free parameters in the fit and common to the K_S^0 and D decay categories. The parameters c_i and s_i are fixed to those determined from the combination of BESIII and CLEO data in ref. [29] for the $D \rightarrow K_S^0 \pi^+ \pi^-$ decays and in ref. [30] for the $D \rightarrow K_S^0 K^+ K^-$ decays. The F_i parameters for each D decay are determined in the fit; separate sets of F_i parameters are determined for the two types of K_S^0 candidates because the efficiency profile over the Dalitz plot differs between the K_S^0 selections. Since the F_i parameters must satisfy the constraints $\sum_i F_i = 1$, $F_i \in [0, 1]$, the fit can suffer from instability if they are included in a naive way due to large correlations. Therefore, the F_i parameters are reparameterised as a series of recursive fractions with parameters, \mathcal{R}_i , determined in the fit. The relation between the F_i and \mathcal{R}_i parameters is given by

$$F_i = \begin{cases} \mathcal{R}_i, & i = -\mathcal{N} \\ \mathcal{R}_i \prod_{j < i} (1 - \mathcal{R}_j), & -\mathcal{N} < i < +\mathcal{N}, \\ \prod_{j < i} (1 - \mathcal{R}_j), & i = +\mathcal{N}. \end{cases} \quad (6.1)$$

for a binning scheme with $2 \times \mathcal{N}$ bins.

The yield of the combinatorial background in each bin is a free parameter. The yield of the partially reconstructed background from B^\pm or B^0 decays in the $B^\pm \rightarrow D\pi^\pm$ and $B^\pm \rightarrow DK^\pm$ samples is also a free parameter in each bin. The composition of the partially reconstructed background is determined from the global fit described in section 5, taking into account the change in the lower limit of invariant mass. The yield of the misidentified partially reconstructed background in the $B^\pm \rightarrow DK^\pm$ samples is determined via the background yield in the corresponding $B^\pm \rightarrow D\pi^\pm$ bin and the relative PID and selection efficiencies. The yield of the $B_s^0 \rightarrow \bar{D}^0 K^- \pi^+$ background is fixed from the global fit and is divided into the Dalitz plot bins according to the F_i such that it has the distribution of a D^0 decay in the B^+ categories and the distribution of a \bar{D}^0 decay in the B^- categories.

There is a small fraction of bins where either the partially reconstructed background or combinatoric background yield is less than one. These bins are identified in a preliminary fit and the background yield is fixed to zero. This procedure is carried out to improve the fit stability.

Pseudoexperiments are performed to investigate any potential biases or remaining instabilities in the fit. The candidate yields and mass distributions in these pseudoexperiments are based on the global fit results. The pull distributions are well described by a Gaussian function and are found to have mean and width consistent with 0 and 1, respectively.

The results for x_\pm^{DK} , y_\pm^{DK} , $x_\xi^{D\pi}$, and $y_\xi^{D\pi}$ are presented in figure 5 along with their likelihood contours, where only statistical uncertainties are considered. The two vectors defined by the origin and the end-point coordinates (x_-^{DK}, y_-^{DK}) and (x_+^{DK}, y_+^{DK}) give the values for r_B^{DK} for B^- and B^+ decays. The signature for CP violation is that these vectors must have non-zero length and have a non-zero opening angle between them, since this angle is equal to 2γ , as illustrated on the figure. Therefore, the data exhibit unambiguous features of CP violation as expected. The relation between the hadronic parameters in $B^\pm \rightarrow D\pi^\pm$ and $B^\pm \rightarrow DK^\pm$ decays is also illustrated in figure 5, where the vector defined by the coordinates $(x_\xi^{D\pi}, y_\xi^{D\pi})$ is the relative magnitude of r_B between the two decay modes. It is consistent with the expectation of 5% [41]. The normalization constants give global asymmetries that are consistent with the expectation of asymmetries from production, detection and neutral kaon effects.

A series of cross checks is carried out by performing separate fits by splitting the data sample into data-taking periods by year, type of K_S^0 candidate, D -decay, hardware trigger path, and magnet polarity. The results are consistent between the datasets. As an additional cross check, the two-stage fit procedure is repeated with a number of different selections applied to the data. Of particular interest are the alternative selections that significantly affect the presence of specific backgrounds: the fits where the value of the BDT threshold is varied to decrease the level of combinatorial background and those where the choice of PID selection is changed to result in a substantially lower level of misidentified $B^\pm \rightarrow D\pi^\pm$ decays and misidentified partially reconstructed background in the $B^\pm \rightarrow DK^\pm$ candidates. The variations in the central values for the CP observables are consistent within the statistical uncertainty associated with the change in the data sample.

In order to assess the goodness of fit and to demonstrate that the equations involving the CP parameters provide a good description of the signal yields in data, an alternative fit

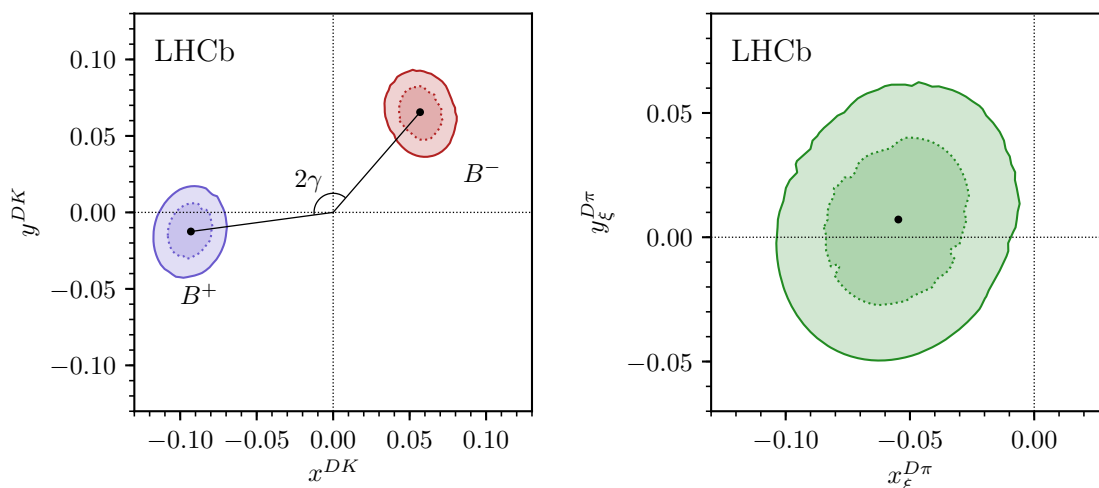


Figure 5. Confidence levels at 68.2% and 95.5% probability for (left, blue) $(x_{\pm}^{DK}, y_{\pm}^{DK})$, (left, red) $(x_{\pm}^{DK}, y_{\pm}^{DK})$, and (right, green) $(x_{\xi}^{D\pi}, y_{\xi}^{D\pi})$ as measured in $B^{\pm} \rightarrow DK^{\pm}$ and $B^{\pm} \rightarrow D\pi^{\pm}$ decays with a profile likelihood scan. The black dots show the central values

is performed where the signal yield in each $B^{\pm} \rightarrow DK^{\pm}$ and $B^{\pm} \rightarrow D\pi^{\pm}$ bin is measured independently. The alternate fit is performed simultaneously in all categories in order to correctly determine the yield of misidentified candidates. These yields are compared with those predicted from the values of $(x_{\pm}^{DK}, y_{\pm}^{DK})$ in the default fit and a high level of agreement is found. In order to visualise the observed CP violation, the asymmetry, $(N_{-i}^{-} - N_{+i}^{+}) / (N_{-i}^{-} + N_{+i}^{+})$, is computed for *effective bin pairs*, defined to comprise bin i for a B^{+} decay and bin $-i$ for a B^{-} decay. Figure 6 shows the obtained asymmetries and those predicted by the values of the CP observables obtained in the fit. A further fit that does not allow for CP violation is carried out by imposing the conditions $x_{+}^{DK} = x_{-}^{DK}$, $y_{+}^{DK} = y_{-}^{DK}$. This determines the predicted asymmetry arising from detector and production effects. In the $B^{\pm} \rightarrow DK^{\pm}$ sample the CP violation is clearly visible as the data are inconsistent with the CP -conserved hypothesis. The observed asymmetries correspond to a $\sim 10\sigma$ deviation given the expectation in the CP -conserving scenario. The predicted asymmetries in the $B^{\pm} \rightarrow D\pi^{\pm}$ decay are an order of magnitude smaller. The data in this analysis cannot distinguish between the CP -violating and CP -conserving predictions for $B^{\pm} \rightarrow D\pi^{\pm}$ due to the relatively large statistical uncertainties.

7 Systematic uncertainties

Systematic uncertainties on the measurements of the CP observables are evaluated and are presented in table 2. The limited precision on (c_i, s_i) coming from the combined BESIII and CLEO [29, 30] results induces uncertainties on the CP parameters. These uncertainties are evaluated by fitting the data multiple times, each time with different $(c_i,$

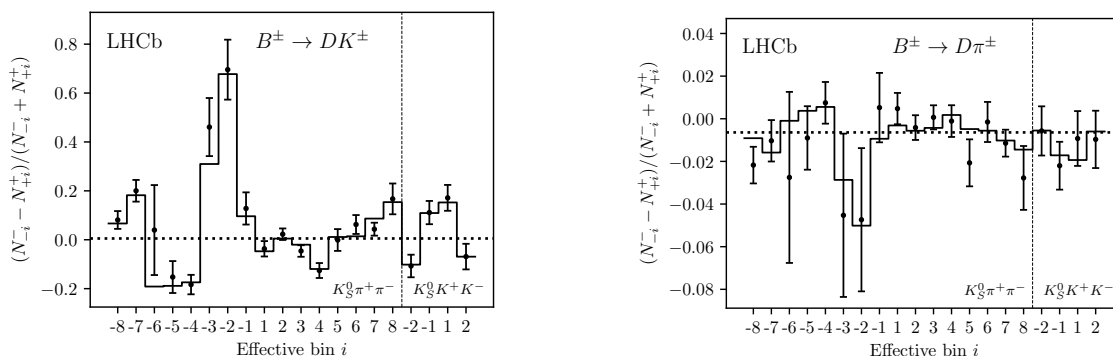


Figure 6. The bin-by-bin asymmetries $(N_{-i}^- - N_{+i}^+) / (N_{-i}^- + N_{+i}^+)$ for each Dalitz-plot bin number for (left) $B^\pm \rightarrow DK^\pm$ decays and (right) $B^\pm \rightarrow D\pi^\pm$ decays. The prediction from the central values of the CP -violation observables is shown with a solid line and the asymmetries obtained in fits with independent bin yields are shown with the error bars. The predicted asymmetries in a fit that does not allow for CP violation are shown with a dotted line. The vertical dashed line separates the $K_S^0\pi^+\pi^-$ and $K_S^0K^+K^-$ bins on the horizontal axis.

Source	$\sigma(x_-^{DK})$	$\sigma(y_-^{DK})$	$\sigma(x_+^{DK})$	$\sigma(y_+^{DK})$	$\sigma(x_\xi^{D\pi})$	$\sigma(y_\xi^{D\pi})$
Statistical	0.96	1.14	0.98	1.23	1.99	2.33
Strong-phase inputs	0.23	0.35	0.18	0.28	0.14	0.18
Efficiency correction of (c_i, s_i)	0.11	0.05	0.05	0.10	0.08	0.09
Mass-shape parameters	0.05	0.08	0.03	0.08	0.16	0.17
PID efficiencies	0.03	0.03	0.01	0.05	0.02	0.02
Fixed yield ratios	0.05	0.06	0.03	0.06	0.02	0.02
Mass-shape bin dependence	0.05	0.07	0.04	0.08	0.07	0.09
Part. reco. physics effects	0.04	0.10	0.15	0.05	0.10	0.09
Small backgrounds	0.11	0.16	0.13	0.12	0.08	0.13
Dalitz-bin migration	0.04	0.08	0.08	0.11	0.18	0.10
CP violation of K_S^0	0.03	0.04	0.08	0.08	0.09	0.46
D mixing	0.04	0.01	0.00	0.02	0.02	0.01
Bias correction	0.04	0.03	0.02	0.04	0.09	0.05
Total LHCb-related uncertainty	0.20	0.25	0.24	0.26	0.32	0.54
Total systematic uncertainty	0.31	0.43	0.30	0.38	0.35	0.57

Table 2. Overview of all sources of uncertainty, σ , on x_\pm^{DK} , y_\pm^{DK} , $x_\xi^{D\pi}$, and $y_\xi^{D\pi}$. All uncertainties are quoted $\times 10^{-2}$.

s_i) values sampled according to their experimental uncertainties and correlations.² The resulting standard deviation of each distribution of the CP observables is assigned as the systematic uncertainty. The size of the systematic uncertainty is notably much smaller than the corresponding uncertainty in ref. [10] due to the improvement in the knowledge of these strong-phase parameters [29, 30].

The non-uniform efficiency profile over the Dalitz plot means that the values of (c_i, s_i) appropriate for this analysis can differ from those measured in refs. [29, 30], which correspond to the case where there is no variation in efficiency over the Dalitz plot. Amplitude models from refs. [46, 67] are used to calculate the values of c_i and s_i both with and without the efficiency profiles determined from simulation. The shift in the c_i and s_i values is taken as an estimate of the size of this effect. Pseudoexperiments are generated assuming the shifted c_i and s_i values and fit with the default values of c_i and s_i . The mean bias of each CP observable is assigned as a systematic uncertainty. The assumption that the relative variation of efficiency over the Dalitz plot is the same in selected $B^\pm \rightarrow DK^\pm$ and $B^\pm \rightarrow D\pi^\pm$ candidates is verified in simulated samples of similar size to the $B^\pm \rightarrow D\pi^\pm$ yields observed in data. No statistically significant difference is observed and no systematic uncertainty is assigned.

The uncertainties from the fixed invariant-mass shapes determined in the global fit are propagated to the CP observables through a resampling method [68]. The following procedure, which takes into account the fact that some parameters are determined in simulation and others in data, is carried out a hundred times. First, the simulated decays that were used to determine the nominal mass shape parameters are each resampled with replacement and fit to determine an alternative set of parameters. Then, the final dataset is resampled with replacement and the global fit is repeated using the alternative fixed shape parameters, to determine alternative values for the parameters that are determined from real data. Finally, the CP fit is performed using the alternative invariant-mass parameterisations, without resampling the final dataset. The standard deviation of the CP observables obtained via this procedure is taken as the systematic uncertainty due to the fixed parameterisation.

The PID efficiencies are varied within their uncertainties in the global and CP fit and the standard deviation of the CP parameters is taken as the systematic uncertainty. A similar method is used to determine the uncertainties due to the fixed fractions between different partially reconstructed backgrounds where the uncertainties on the fixed fractions are those from the branching fractions [60] and the selection efficiencies.

The CP fit assumes the same mass shape for each component in each Dalitz plot bin. For the signal and cross-feed backgrounds the shapes are redetermined in each bin using the same procedures described in section 5. The variance is very small due to weak correlations between phase-space coordinates and particle kinematics. The combinatorial slope can also vary from bin to bin, as the relative rate of combinatorial background with and without a real D^0 meson will not be constant. The size of this effect is determined through the study of the high invariant-mass sideband where only combinatorial background contributes.

²The detailed output of this study is available as [supplementary material](#) to this paper, and provides sufficient information to determine the correlation between this uncertainty and the corresponding uncertainties of future γ measurements that also rely on the same strong-phase measurements.

Pseudodata are generated where this variation in mass shape across the Dalitz plot bins is replicated for signal, cross-feed and combinatorial backgrounds, and the generated samples are fit with the default fit assumptions of the same shape in each bin. The mean bias is assigned as the systematic uncertainty.

The partially reconstructed background shape is also expected to vary in each bin, however the leading source of this effect is due to the individual components of this background having a different distribution over the Dalitz plot. Some partially reconstructed backgrounds will be distributed as D^0 (\bar{D}^0) $\rightarrow D \rightarrow K_S^0 h^+ h^-$ for reconstructed B^- (B^+) candidates, while others will be distributed as a D^0 - \bar{D}^0 admixture depending on the relevant CP -violation parameters. Pseudodata are generated, where the D -decay phase-space distributions for $B^\pm \rightarrow D^* K^\pm$ and $B^\pm \rightarrow DK^{*\pm}$ background events are based on the CP parameters reported in ref. [69]. No CP violation is introduced into the partially reconstructed background in the $B^\pm \rightarrow D\pi^\pm$ samples since it is expected to be small, and the $B^0 \rightarrow D\rho^0$ background is treated as an equal mix of D^0 and \bar{D}^0 since either pion can be reconstructed. The generated pseudodata are fitted with the default fit and the mean bias is assigned as the systematic uncertainty.

Systematic uncertainties are assigned for small residual backgrounds that contaminate the data sample but are not accounted for in the fit. Their impact is assessed by generating pseudoexperiments that contain these backgrounds and are fit with the default model. The mean bias is assigned as the uncertainty. One source of background is from $\Lambda_b^0 \rightarrow Dp\pi^-$ decays where the pion is not reconstructed and the proton is misidentified as a kaon. This background is modelled as a \bar{D}^0 -like contribution in B^- decays, and has an expected yield of 0.5% of the $B^\pm \rightarrow DK^\pm$ signal. A further, even smaller, background is $\Lambda_c^0 \rightarrow \Lambda_c^+(\rightarrow pK_S^0\pi^+\pi^-)\pi^-$ decays where the π^+ meson in the Λ_c^+ decay is missed, and the p reconstructed as the π^+ from the D -decay. The effective distribution of the reconstructed D meson is unknown and is assigned to be \bar{D}^0 -like in B^- decays to be conservative. The mass shapes and rates of these backgrounds are determined from simulation. Another source of background comes from residual $B \rightarrow D\mu\nu$ decays, where the rate (less than 0.2% relative to the signal mode, after the applied veto) and shape are determined from simulation with PID efficiencies from calibration data. The residual semileptonic D decay background has a rate of less than 0.1% of signal and the distribution of these events on the Dalitz plot is determined through a simplified simulation [59] taking into account various K^* mesons. Finally, a small peaking background from $B^\pm \rightarrow D(\rightarrow K^\pm\pi^\mp)K_S^0\pi^\pm$ decays where the kaon is reconstructed as the companion and the other particles are assigned to the D decay is considered. The yield of this background is determined to be 0.5% of the signal yield in $B^\pm \rightarrow DK^\pm$ by a data driven study of the invariant-mass distribution of switched tracks. The distribution on the Dalitz plot is determined through the simplified simulation [59] where different $K^{*\pm} \rightarrow K_S^0\pi^\pm$ resonances are generated.

The main effect of migration from one Dalitz plot bin to another is implicitly taken into account by using the data to determine the F_i , which thus include the effects of the net bin migration. However, a small effect arises because of the differences in the distributions of the $B^\pm \rightarrow DK^\pm$ and $B^\pm \rightarrow D\pi^\pm$ decays due to the differing hadronic decay parameters. To investigate this, data points are generated according to the amplitude model in ref. [67]

with CP observables consistent with expectation [5, 69]. To smear these data points on the Dalitz plot, an event is selected from full LHCb simulation and the difference in m_+^2 and m_-^2 between its true and reconstructed quantities is applied to the data point in order to determine its reconstructed bin. The difference between true and reconstructed quantities is multiplied by a factor of 1.2 to account for differences in resolution between data and simulation. Pseudoexperiments are generated based on the expected reconstructed yields in each bin and fit with a nominal fit where the c_i and s_i parameters are determined by the amplitude model [67]. The mean bias in the CP violation parameters is taken as the systematic uncertainty, which is small.

The impact of ignoring the CP violation and matter effects in K_S^0 decays is determined through generating pseudoexperiments taking into account all these effects as detailed in ref. [39], where LHCb simulation is used to obtain the K_S^0 lifetime acceptance and momentum distribution. The size of the bias found is consistent with those expected from ref. [39], where it was also predicted that the relative uncertainties on $B^\pm \rightarrow D\pi^\pm$ observables are expected to be larger than for $B^\pm \rightarrow DK^\pm$ observables. This is found to be true, but even the most significant uncertainty, on $y_\xi^{D\pi}$, is an order of magnitude smaller than the corresponding statistical uncertainty. The effect of ignoring charm mixing is expected to be minimal, given that the first-order effects are inherently taken into account when the F_i parameters are measured as a part of the fit [38]. This is verified by generating pseudoexperiments that include charm mixing and fitting them with the nominal fit.

In previous studies, a bias correction has been necessary when similar measurements have been performed with lower signal yields [10] leading to some fit instabilities. In this case, the higher yields have resulted in a bias that is of negligible size and hence no correction is applied. Nonetheless, the uncertainty on the biases are assigned as the systematic uncertainties.

In general, all the systematic uncertainties are small in comparison to the statistical uncertainties. There is no dominant source of systematic uncertainty for all CP observables, however the description of backgrounds, either those not modelled or the modelling of the partially reconstructed backgrounds are some of the larger sources. The uncertainty attributed to the precision of the strong-phase measurements is of similar size to the total LHCb-related systematic uncertainty.

8 Interpretation

The CP observables are measured to be

$$\begin{aligned}
 x_-^{DK} &= (5.68 \pm 0.96 \pm 0.20 \pm 0.23) \times 10^{-2}, \\
 y_-^{DK} &= (6.55 \pm 1.14 \pm 0.25 \pm 0.35) \times 10^{-2}, \\
 x_+^{DK} &= (-9.30 \pm 0.98 \pm 0.24 \pm 0.18) \times 10^{-2}, \\
 y_+^{DK} &= (-1.25 \pm 1.23 \pm 0.26 \pm 0.28) \times 10^{-2}, \\
 x_\xi^{D\pi} &= (-5.47 \pm 1.99 \pm 0.32 \pm 0.14) \times 10^{-2}, \\
 y_\xi^{D\pi} &= (0.71 \pm 2.33 \pm 0.54 \pm 0.18) \times 10^{-2},
 \end{aligned}
 \tag{8.1}$$

where the first uncertainty is statistical, the second arises from systematic effects in the method or detector considerations, and the third from external inputs of strong-phase measurements from the combination of CLEO and BESIII [27, 29] results. The correlation matrices for each source of uncertainty are available in the appendices in tables 3–5.

The CP observables are interpreted in terms of the underlying physics parameters γ , and r_B and δ_B for each B^\pm decay mode. The interpretation is done via a maximum likelihood fit using a frequentist treatment as described in ref. [44]. The solution for the physics parameters has a two-fold ambiguity as the equations are invariant under the simultaneous substitutions $\gamma \rightarrow \gamma + 180^\circ$ and $\delta_B \rightarrow \delta_B + 180^\circ$. The solution that satisfies $0 < \gamma < 180^\circ$ is chosen, and leads to

$$\begin{aligned}
 \gamma &= (68.7_{-5.1}^{+5.2})^\circ, \\
 r_B^{DK^\pm} &= 0.0904_{-0.0075}^{+0.0077}, \\
 \delta_B^{DK^\pm} &= (118.3_{-5.6}^{+5.5})^\circ, \\
 r_B^{D\pi^\pm} &= 0.0050 \pm 0.0017, \\
 \delta_B^{D\pi^\pm} &= (291_{-26}^{+24})^\circ.
 \end{aligned}
 \tag{8.2}$$

Pseudoexperiments are carried out to confirm that the value of γ is extracted without bias. This is the most precise single measurement of γ to date. The result is consistent with the indirect determination $\gamma = (65.66_{-2.65}^{+0.90})^\circ$ [6]. The confidence limits for γ are illustrated in figure 7, while figure 8 shows the two-dimensional confidence regions obtained for the (γ, r_B) and (r_B, δ_B) parameter combinations. The results for γ , r_B^{DK} , and δ_B^{DK} are consistent with their current world averages [5, 6] which include the LHCb results obtained with the 2011–2016 data. The knowledge of $r_B^{D\pi}$ and $\delta_B^{D\pi}$ from other sources is limited, with the combination of many observables presented in ref. [44] providing two possible solutions. The results here have a single solution, and favour a central value that is consistent with the expectation for $r_B^{D\pi}$, given the value of r_B^{DK} and CKM elements [41]. This is likely to remove the two-solution aspect in future combinations of γ and associated hadronic parameters. The low value of $r_B^{D\pi}$ means that the direct contribution to γ from $B^\pm \rightarrow D\pi^\pm$ decays in this measurement is minimal. However the ability to use this decay mode to determine the efficiency has approximately halved the total LHCb related experimental systematic uncertainty in comparison to ref. [10]. The new inputs from the BESIII collaboration have led to the strong-phase related uncertainty on γ to be approximately 1° , which is a significant reduction compared to the propagated uncertainty when only CLEO measurements were available.

9 Conclusions

In summary, the decays $B^\pm \rightarrow DK^\pm$ and $B^\pm \rightarrow D\pi^\pm$ with $D \rightarrow K_S^0\pi^+\pi^-$ or $D \rightarrow K_S^0K^+K^-$ obtained from the full LHCb dataset collected to date, corresponding to an integrated luminosity of 9 fb^{-1} , have been analysed to determine the CKM angle γ . The sensitivity to γ comes almost entirely from $B^\pm \rightarrow DK^\pm$ decays where the signal yields of reconstructed events are approximately 13600 (1900) in the $D \rightarrow K_S^0\pi^+\pi^-$ ($D \rightarrow K_S^0K^+K^-$)

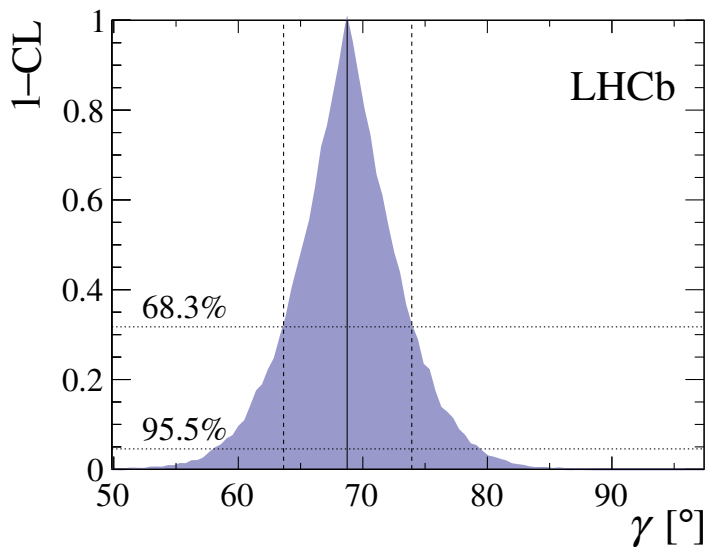


Figure 7. Confidence limits for the CKM angle γ obtained using the method described in ref. [44].

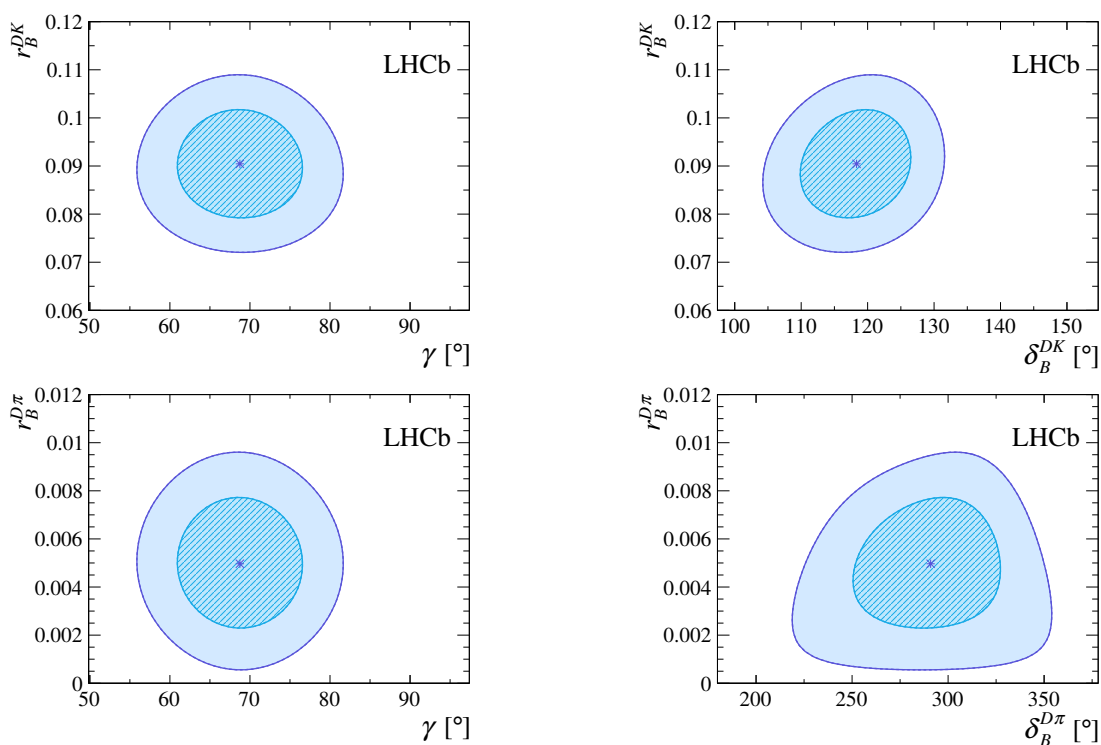


Figure 8. The 68% and 95% confidence regions for combinations of the physics parameters $(\gamma, r_B^{DK}, \delta_B^{DK}, r_B^{D\pi}, \delta_B^{D\pi})$ obtained using the methods described in ref. [44].

decay modes. The $B^\pm \rightarrow D\pi^\pm$ data is primarily used to control effects due to selection and reconstruction of the data, which leads to small experimental systematic uncertainties. The analysis is performed in bins of the D -decay Dalitz plot and a combination of measurements performed by the CLEO and BESIII collaborations presented in refs. [29, 30] are used to provide input on the D -decay strong-phase parameters (c_i, s_i) . Such an approach allows the analysis to be free from model-dependent assumptions on the strong-phase variation across the Dalitz plot. The analysis also determines the hadronic parameters r_B and δ_B for each B^\pm decay mode. Those of the $B^\pm \rightarrow DK^\pm$ decay are consistent with current averages, and those of the $B^\pm \rightarrow D\pi^\pm$ decay are obtained with the best precision to date, and have not previously been measured using these D -decay modes. The CKM angle γ is determined to be $\gamma = (68.7_{-5.1}^{+5.2})^\circ$, where the result is limited by statistical uncertainties. This is the most precise measurement of γ from a single analysis, and supersedes the results in refs. [10, 31].

Acknowledgments

We express our gratitude to our colleagues in the CERN accelerator departments for the excellent performance of the LHC. We thank the technical and administrative staff at the LHCb institutes. We acknowledge support from CERN and from the national agencies: CAPES, CNPq, FAPERJ and FINEP (Brazil); MOST and NSFC (China); CNRS/IN2P3 (France); BMBF, DFG and MPG (Germany); INFN (Italy); NWO (Netherlands); MNiSW and NCN (Poland); MEN/IFA (Romania); MSHE (Russia); MICINN (Spain); SNSF and SER (Switzerland); NASU (Ukraine); STFC (United Kingdom); DOE NP and NSF (U.S.A.). We acknowledge the computing resources that are provided by CERN, IN2P3 (France), KIT and DESY (Germany), INFN (Italy), SURF (Netherlands), PIC (Spain), GridPP (United Kingdom), RRCKI and Yandex LLC (Russia), CSCS (Switzerland), IFIN-HH (Romania), CBPF (Brazil), PL-GRID (Poland) and OSC (U.S.A.). We are indebted to the communities behind the multiple open-source software packages on which we depend. Individual groups or members have received support from AvH Foundation (Germany); EPLANET, Marie Skłodowska-Curie Actions and ERC (European Union); A*MIDEX, ANR, Labex P2IO and OCEVU, and Région Auvergne-Rhône-Alpes (France); Key Research Program of Frontier Sciences of CAS, CAS PIFI, Thousand Talents Program, and Sci. & Tech. Program of Guangzhou (China); RFBR, RSF and Yandex LLC (Russia); GVA, XuntaGal and GENCAT (Spain); the Royal Society and the Leverhulme Trust (United Kingdom).

A Correlation matrices

The correlations matrices for the measured observables are shown in tables 3–5 for the statistical uncertainties, the experimental systematic uncertainties, and the strong-phase-related uncertainties, respectively.

Uncertainty ($\times 10^{-2}$)						
	x_-^{DK}	y_-^{DK}	x_+^{DK}	y_+^{DK}	$x_\xi^{D\pi}$	$y_\xi^{D\pi}$
σ	0.96	1.14	0.98	1.23	1.99	2.33

Correlation matrix						
	x_-^{DK}	y_-^{DK}	x_+^{DK}	y_+^{DK}	$x_\xi^{D\pi}$	$y_\xi^{D\pi}$
x_-^{DK}	1	-0.125	-0.013	0.019	0.037	-0.161
y_-^{DK}		1	-0.011	-0.010	0.097	0.041
x_+^{DK}			1	0.105	-0.108	0.032
y_+^{DK}				1	-0.070	-0.147
$x_\xi^{D\pi}$					1	0.150
$y_\xi^{D\pi}$						1

Table 3. Statistical uncertainties, σ , and correlation matrix for x_\pm^{DK} , y_\pm^{DK} , $x_\xi^{D\pi}$, and $y_\xi^{D\pi}$.

Uncertainty ($\times 10^{-2}$)						
	x_-^{DK}	y_-^{DK}	x_+^{DK}	y_+^{DK}	$x_\xi^{D\pi}$	$y_\xi^{D\pi}$
σ	0.20	0.25	0.24	0.26	0.32	0.54

Correlation matrix						
	x_-^{DK}	y_-^{DK}	x_+^{DK}	y_+^{DK}	$x_\xi^{D\pi}$	$y_\xi^{D\pi}$
x_-^{DK}	1	0.864	0.734	0.897	0.349	0.318
y_-^{DK}		1	0.874	0.903	0.408	0.362
x_+^{DK}			1	0.771	0.563	0.447
y_+^{DK}				1	0.507	0.451
$x_\xi^{D\pi}$					1	0.484
$y_\xi^{D\pi}$						1

Table 4. Total LHCb-related systematic uncertainties, σ , for x_\pm^{DK} , y_\pm^{DK} , $x_\xi^{D\pi}$, and $y_\xi^{D\pi}$, and the corresponding correlation matrix.

Uncertainty ($\times 10^{-2}$)						
	x_-^{DK}	y_-^{DK}	x_+^{DK}	y_+^{DK}	$x_\xi^{D\pi}$	$y_\xi^{D\pi}$
σ	0.23	0.35	0.18	0.28	0.14	0.18

Correlation matrix						
	x_-^{DK}	y_-^{DK}	x_+^{DK}	y_+^{DK}	$x_\xi^{D\pi}$	$y_\xi^{D\pi}$
x_-^{DK}	1	-0.047	-0.490	0.322	0.189	0.144
y_-^{DK}		1	0.059	-0.237	-0.116	-0.117
x_+^{DK}			1	0.061	0.004	-0.139
y_+^{DK}				1	0.127	-0.199
$x_\xi^{D\pi}$					1	0.638
$y_\xi^{D\pi}$						1

Table 5. Systematic uncertainties, σ , for x_\pm^{DK} , y_\pm^{DK} , $x_\xi^{D\pi}$, and $y_\xi^{D\pi}$ due to strong-phase inputs, the corresponding correlation matrix.

Open Access. This article is distributed under the terms of the Creative Commons Attribution License ([CC-BY 4.0](https://creativecommons.org/licenses/by/4.0/)), which permits any use, distribution and reproduction in any medium, provided the original author(s) and source are credited.

References

- [1] N. Cabibbo, *Unitary symmetry and leptonic decays*, *Phys. Rev. Lett.* **10** (1963) 531 [[INSPIRE](#)].
- [2] M. Kobayashi and T. Maskawa, *CP violation in the renormalizable theory of weak interaction*, *Prog. Theor. Phys.* **49** (1973) 652 [[INSPIRE](#)].
- [3] J. Brod and J. Zupan, *The ultimate theoretical error on γ from $B \rightarrow DK$ decays*, *JHEP* **01** (2014) 051 [[arXiv:1308.5663](#)] [[INSPIRE](#)].
- [4] M. Blanke and A.J. Buras, *Emerging ΔM_d -anomaly from tree-level determinations of $|V_{cb}|$ and the angle γ* , *Eur. Phys. J. C* **79** (2019) 159 [[arXiv:1812.06963](#)] [[INSPIRE](#)].
- [5] HFLAV collaboration, *Averages of b-hadron, c-hadron, and τ -lepton properties as of 2018*, [arXiv:1909.12524](#) [[INSPIRE](#)].
- [6] CKMFITTER GROUP collaboration, *CP violation and the CKM matrix: assessing the impact of the asymmetric B factories*, *Eur. Phys. J. C* **41** (2005) 1 [[hep-ph/0406184](#)] [[INSPIRE](#)].
- [7] LHCb collaboration, *Measurement of CP observables in $B^\pm \rightarrow DK^\pm$ and $B^\pm \rightarrow D\pi^\pm$ with $D \rightarrow K_S^0 K^\pm \pi^\mp$ decays*, *JHEP* **06** (2020) 058 [[arXiv:2002.08858](#)] [[INSPIRE](#)].
- [8] LHCb collaboration, *Measurement of CP observables in $B^\pm \rightarrow DK^\pm$ and $B^\pm \rightarrow D\pi^\pm$ with two- and four-body D decays*, *Phys. Lett. B* **760** (2016) 117 [[arXiv:1603.08993](#)] [[INSPIRE](#)].

- [9] LHCb collaboration, *A study of CP violation in $B^\mp \rightarrow Dh^\mp$ ($h = K, \pi$) with the modes $D \rightarrow K^\mp \pi^\pm \pi^0$, $D \rightarrow \pi^+ \pi^- \pi^0$ and $D \rightarrow K^+ K^- \pi^0$* , *Phys. Rev. D* **91** (2015) 112014 [[arXiv:1504.05442](#)] [[INSPIRE](#)].
- [10] LHCb collaboration, *Measurement of the CKM angle γ using $B^\pm \rightarrow DK^\pm$ with $D \rightarrow K_S^0 \pi^+ \pi^-$, $K_S^0 K^+ K^-$ decays*, *JHEP* **08** (2018) 176 [Erratum *ibid.* **10** (2018) 107] [[arXiv:1806.01202](#)] [[INSPIRE](#)].
- [11] BELLE collaboration, *First measurement of the CKM angle ϕ_3 with $B^\pm \rightarrow D(K_S^0 \pi^+ \pi^- \pi^0) K^\pm$ decays*, *JHEP* **10** (2019) 178 [[arXiv:1908.09499](#)] [[INSPIRE](#)].
- [12] D. Atwood, I. Dunietz and A. Soni, *Enhanced CP-violation with $B \rightarrow KD^0(\bar{D}^0)$ modes and extraction of the CKM angle gamma*, *Phys. Rev. Lett.* **78** (1997) 3257 [[hep-ph/9612433](#)] [[INSPIRE](#)].
- [13] D. Atwood, I. Dunietz and A. Soni, *Improved methods for observing CP-violation in $B^\pm \rightarrow KD$ and measuring the CKM phase gamma*, *Phys. Rev. D* **63** (2001) 036005 [[hep-ph/0008090](#)] [[INSPIRE](#)].
- [14] M. Gronau and D. Wyler, *On determining a weak phase from CP asymmetries in charged B decays*, *Phys. Lett. B* **265** (1991) 172 [[INSPIRE](#)].
- [15] M. Gronau and D. London, *How to determine all the angles of the unitarity triangle from $B_d^0 \rightarrow DK_s$ and $B_s^0 \rightarrow D_\varphi$* , *Phys. Lett. B* **253** (1991) 483 [[INSPIRE](#)].
- [16] M. Nayak et al., *First determination of the CP content of $D \rightarrow \pi^+ \pi^- \pi^0$ and $D \rightarrow K^+ K^- \pi^0$* , *Phys. Lett. B* **740** (2015) 1 [[arXiv:1410.3964](#)] [[INSPIRE](#)].
- [17] A. Giri, Y. Grossman, A. Soffer and J. Zupan, *Determining gamma using $B^\pm \rightarrow DK^\pm$ with multibody D decays*, *Phys. Rev. D* **68** (2003) 054018 [[hep-ph/0303187](#)] [[INSPIRE](#)].
- [18] A. Bondar, *Proceedings of BINP special analysis meeting on Dalitz analysis*, unpublished, 24–26 September 2002.
- [19] BELLE collaboration, *Measurement of ϕ_3 with Dalitz plot analysis of $B^\pm \rightarrow D^{(*)} K^\pm$ decay*, *Phys. Rev. D* **70** (2004) 072003 [[hep-ex/0406067](#)] [[INSPIRE](#)].
- [20] Y. Grossman, Z. Ligeti and A. Soffer, *Measuring gamma in $B^\pm \rightarrow K^\pm(KK^*)_D$ decays*, *Phys. Rev. D* **67** (2003) 071301 [[hep-ph/0210433](#)] [[INSPIRE](#)].
- [21] LHCb collaboration, *Model-independent measurement of the CKM angle γ using $B^0 \rightarrow DK^{*0}$ decays with $D \rightarrow K_S^0 \pi^+ \pi^-$ and $K_S^0 K^+ K^-$* , *JHEP* **06** (2016) 131 [[arXiv:1604.01525](#)] [[INSPIRE](#)].
- [22] LHCb collaboration, *Measurement of CP observables in $B^\pm \rightarrow DK^{*\pm}$ decays using two- and four-body D final states*, *JHEP* **11** (2017) 156 [Erratum *ibid.* **05** (2018) 067] [[arXiv:1709.05855](#)] [[INSPIRE](#)].
- [23] LHCb collaboration, *Study of $B^- \rightarrow DK^- \pi^+ \pi^-$ and $B^- \rightarrow D \pi^- \pi^+ \pi^-$ decays and determination of the CKM angle γ* , *Phys. Rev. D* **92** (2015) 112005 [[arXiv:1505.07044](#)] [[INSPIRE](#)].
- [24] LHCb collaboration, *Measurement of CP observables in $B^\pm \rightarrow D^{(*)} K^\pm$ and $B^\pm \rightarrow D^{(*)} \pi^\pm$ decays*, *Phys. Lett. B* **777** (2018) 16 [[arXiv:1708.06370](#)] [[INSPIRE](#)].
- [25] A. Bondar and A. Poluektov, *Feasibility study of model-independent approach to ϕ_3 measurement using Dalitz plot analysis*, *Eur. Phys. J. C* **47** (2006) 347 [[hep-ph/0510246](#)] [[INSPIRE](#)].

- [26] A. Bondar and A. Poluektov, *The use of quantum-correlated D^0 decays for ϕ_3 measurement*, *Eur. Phys. J. C* **55** (2008) 51 [[arXiv:0801.0840](#)] [[INSPIRE](#)].
- [27] CLEO collaboration, *Model-independent determination of the strong-phase difference between D^0 and $\bar{D}^0 \rightarrow K_{S,L}^0 h^+ h^-$ ($h = \pi, K$) and its impact on the measurement of the CKM angle γ/ϕ_3* , *Phys. Rev. D* **82** (2010) 112006 [[arXiv:1010.2817](#)] [[INSPIRE](#)].
- [28] BESIII collaboration, *Determination of strong-phase parameters in $D \rightarrow K_{S,L}^0 \pi^+ \pi^-$* , *Phys. Rev. Lett.* **124** (2020) 241802 [[arXiv:2002.12791](#)] [[INSPIRE](#)].
- [29] BESIII collaboration, *Model-independent determination of the relative strong-phase difference between D^0 and $\bar{D}^0 \rightarrow K_{S,L}^0 \pi^+ \pi^-$ and its impact on the measurement of the CKM angle γ/ϕ_3* , *Phys. Rev. D* **101** (2020) 112002 [[arXiv:2003.00091](#)] [[INSPIRE](#)].
- [30] BESIII collaboration, *Improved model-independent determination of the strong-phase difference between D^0 and $\bar{D}^0 \rightarrow K_{S,L}^0 K^+ K^-$ decays*, *Phys. Rev. D* **102** (2020) 052008 [[arXiv:2007.07959](#)] [[INSPIRE](#)].
- [31] LHCb collaboration, *Measurement of the CKM angle γ using $B^\pm \rightarrow DK^\pm$ with $D \rightarrow K_S^0 \pi^+ \pi^-$, $K_S^0 K^+ K^-$ decays*, *JHEP* **10** (2014) 097 [[arXiv:1408.2748](#)] [[INSPIRE](#)].
- [32] BELLE collaboration, *First measurement of ϕ_3 with a model-independent Dalitz plot analysis of $B^\pm \rightarrow DK$, $D \rightarrow K_s^0 \pi \pi$ decay*, *Phys. Rev. D* **85** (2012) 112014 [[arXiv:1204.6561](#)] [[INSPIRE](#)].
- [33] BELLE collaboration, *First model-independent Dalitz analysis of $B^0 \rightarrow DK^{*0}$, $D \rightarrow K_S^0 \pi^+ \pi^-$ decay*, *PTEP* **2016** (2016) 043C01 [[arXiv:1509.01098](#)] [[INSPIRE](#)].
- [34] BABAR collaboration, *Evidence for direct CP-violation in the measurement of the Cabibbo-Kobayashi-Maskawa angle gamma with $B^\mp \rightarrow D^{(*)} K^{(*)\mp}$ decays*, *Phys. Rev. Lett.* **105** (2010) 121801 [[arXiv:1005.1096](#)] [[INSPIRE](#)].
- [35] BELLE collaboration, *Evidence for direct CP-violation in the decay $B \rightarrow D^{(*)} K$, $D \rightarrow K_s \pi^+ \pi^-$ and measurement of the CKM phase ϕ_3* , *Phys. Rev. D* **81** (2010) 112002 [[arXiv:1003.3360](#)] [[INSPIRE](#)].
- [36] LHCb collaboration, *Measurement of CP violation and constraints on the CKM angle γ in $B^\pm \rightarrow DK^\pm$ with $D \rightarrow K_S^0 \pi^+ \pi^-$ decays*, *Nucl. Phys. B* **888** (2014) 169 [[arXiv:1407.6211](#)] [[INSPIRE](#)].
- [37] M. Battaglieri et al., *Analysis tools for next-generation hadron spectroscopy experiments*, *Acta Phys. Polon. B* **46** (2015) 257 [[arXiv:1412.6393](#)] [[INSPIRE](#)].
- [38] A. Bondar, A. Poluektov and V. Vorobiev, *Charm mixing in the model-independent analysis of correlated $D^0 \bar{D}^0$ decays*, *Phys. Rev. D* **82** (2010) 034033 [[arXiv:1004.2350](#)] [[INSPIRE](#)].
- [39] M. Bjørn and S. Malde, *CP violation and material interaction of neutral kaons in measurements of the CKM angle γ using $B^\pm \rightarrow DK^\pm$ decays where $D \rightarrow K_S^0 \pi^+ \pi^-$* , *JHEP* **07** (2019) 106 [[arXiv:1904.01129](#)] [[INSPIRE](#)].
- [40] BABAR collaboration, *Measurement of γ in $B^\mp \rightarrow D^{(*)} K^\mp$ decays with a Dalitz analysis of $D \rightarrow K_S^0 \pi^- \pi^+$* , *Phys. Rev. Lett.* **95** (2005) 121802 [[hep-ex/0504039](#)] [[INSPIRE](#)].
- [41] M. Kenzie, M. Martinelli and N. Tuning, *Estimating $r_B^{D\pi}$ as an input to the determination of the CKM angle γ* , *Phys. Rev. D* **94** (2016) 054021 [[arXiv:1606.09129](#)] [[INSPIRE](#)].
- [42] J. Garra Ticó, *A strategy for a simultaneous measurement of CP violation parameters related to the CKM angle γ in multiple B meson decay channels*, [arXiv:1804.05597](#) [[INSPIRE](#)].

- [43] J. Garra Tico, V. Gibson, S.C. Haines, C.R. Jones, M. Kenzie and G. Lovell, *Study of the sensitivity to CKM angle γ under simultaneous determination from multiple B meson decay modes*, *Phys. Rev. D* **102** (2020) 053003 [[arXiv:1909.00600](#)] [[INSPIRE](#)].
- [44] LHCb collaboration, *Measurement of the CKM angle γ from a combination of LHCb results*, *JHEP* **12** (2016) 087 [[arXiv:1611.03076](#)] [[INSPIRE](#)].
- [45] BABAR collaboration, *Improved measurement of the CKM angle γ in $B^\mp \rightarrow D^{(*)}K^{(*)\mp}$ decays with a Dalitz plot analysis of D decays to $K_S^0\pi^+\pi^-$ and $K_S^0K^+K^-$* , *Phys. Rev. D* **78** (2008) 034023 [[arXiv:0804.2089](#)] [[INSPIRE](#)].
- [46] BABAR collaboration, *Evidence for direct CP-violation in the measurement of the Cabibbo-Kobayashi-Maskawa angle gamma with $B^\mp \rightarrow D^{(*)}K^{(*)\mp}$ decays*, *Phys. Rev. Lett.* **105** (2010) 121801 [[arXiv:1005.1096](#)] [[INSPIRE](#)].
- [47] LHCb collaboration, *The LHCb detector at the LHC*, *2008 JINST* **3** S08005 [[INSPIRE](#)].
- [48] LHCb collaboration, *LHCb detector performance*, *Int. J. Mod. Phys. A* **30** (2015) 1530022 [[arXiv:1412.6352](#)] [[INSPIRE](#)].
- [49] V.V. Gligorov and M. Williams, *Efficient, reliable and fast high-level triggering using a bonsai boosted decision tree*, *2013 JINST* **8** P02013 [[arXiv:1210.6861](#)] [[INSPIRE](#)].
- [50] T. Sjöstrand, S. Mrenna and P.Z. Skands, *A brief introduction to PYTHIA 8.1*, *Comput. Phys. Commun.* **178** (2008) 852 [[arXiv:0710.3820](#)] [[INSPIRE](#)].
- [51] T. Sjöstrand, S. Mrenna and P.Z. Skands, *PYTHIA 6.4 physics and manual*, *JHEP* **05** (2006) 026 [[hep-ph/0603175](#)] [[INSPIRE](#)].
- [52] LHCb collaboration, *Handling of the generation of primary events in Gauss, the LHCb simulation framework*, *J. Phys. Conf. Ser.* **331** (2011) 032047 [[INSPIRE](#)].
- [53] D.J. Lange, *The EvtGen particle decay simulation package*, *Nucl. Instrum. Meth. A* **462** (2001) 152 [[INSPIRE](#)].
- [54] P. Golonka and Z. Was, *PHOTOS Monte Carlo: a precision tool for QED corrections in Z and W decays*, *Eur. Phys. J. C* **45** (2006) 97 [[hep-ph/0506026](#)] [[INSPIRE](#)].
- [55] J. Allison et al., *GEANT4 developments and applications*, *IEEE Trans. Nucl. Sci.* **53** (2006) 270 [[INSPIRE](#)].
- [56] GEANT4 collaboration, *GEANT4 — a simulation toolkit*, *Nucl. Instrum. Meth. A* **506** (2003) 250 [[INSPIRE](#)].
- [57] LHCb collaboration, *The LHCb simulation application, Gauss: design, evolution and experience*, *J. Phys. Conf. Ser.* **331** (2011) 032023 [[INSPIRE](#)].
- [58] D. Müller, M. Clemencic, G. Corti and M. Gersabeck, *ReDecay: a novel approach to speed up the simulation at LHCb*, *Eur. Phys. J. C* **78** (2018) 1009 [[arXiv:1810.10362](#)] [[INSPIRE](#)].
- [59] G.A. Cowan, D.C. Craik and M.D. Needham, *RapidSim: an application for the fast simulation of heavy-quark hadron decays*, *Comput. Phys. Commun.* **214** (2017) 239 [[arXiv:1612.07489](#)] [[INSPIRE](#)].
- [60] PARTICLE DATA GROUP collaboration, *Review of particle physics*, *PTEP* **2020** (2020) 083C01 [[INSPIRE](#)].
- [61] L. Breiman, J.H. Friedman, R.A. Olshen and C.J. Stone, *Classification and regression trees*, Wadsworth international group, Belmont, CA, U.S.A. (1984) [[INSPIRE](#)].

- [62] Y. Freund and R.E. Schapire, *A decision-theoretic generalization of on-line learning and an application to boosting*, *J. Comput. Syst. Sci.* **55** (1997) 119.
- [63] W.D. Hulsbergen, *Decay chain fitting with a Kalman filter*, *Nucl. Instrum. Meth. A* **552** (2005) 566 [[physics/0503191](#)] [[INSPIRE](#)].
- [64] LHCb collaboration, *Constraints on the unitarity triangle angle γ from Dalitz plot analysis of $B^0 \rightarrow DK^+\pi^-$ decays*, *Phys. Rev. D* **93** (2016) 112018 [*Erratum ibid.* **94** (2016) 079902] [[arXiv:1602.03455](#)] [[INSPIRE](#)].
- [65] LHCb collaboration, *Dalitz plot analysis of $B_s^0 \rightarrow \bar{D}^0 K^- \pi^+$ decays*, *Phys. Rev. D* **90** (2014) 072003 [[arXiv:1407.7712](#)] [[INSPIRE](#)].
- [66] LHCb collaboration, *Measurement of b hadron fractions in 13 TeV pp collisions*, *Phys. Rev. D* **100** (2019) 031102 [[arXiv:1902.06794](#)] [[INSPIRE](#)].
- [67] BABAR and BELLE collaborations, *Measurement of $\cos 2\beta$ in $B^0 \rightarrow D^{(*)}h^0$ with $D \rightarrow K_S^0 \pi^+ \pi^-$ decays by a combined time-dependent Dalitz plot analysis of BaBar and Belle data*, *Phys. Rev. D* **98** (2018) 112012 [[arXiv:1804.06153](#)] [[INSPIRE](#)].
- [68] M.R. Chernick, *Bootstrap methods: a practitioner's guide*, Wiley-Interscience publication, U.S.A. (1999).
- [69] LHCb collaboration, *Update of the LHCb combination of the CKM angle γ* , Tech. Rep. [LHCb-CONF-2018-002](#), CERN, Geneva, Switzerland (2018).

The LHCb collaboration

R. Aaij³¹, C. Abellán Beteta⁴⁹, T. Ackernley⁵⁹, B. Adeva⁴⁵, M. Adinolfi⁵³, H. Afsharnia⁹, C.A. Aidala⁸⁴, S. Aiola²⁵, Z. Ajaltouni⁹, S. Akar⁶⁴, J. Albrecht¹⁴, F. Alessio⁴⁷, M. Alexander⁵⁸, A. Alfonso Albero⁴⁴, Z. Aliouche⁶¹, G. Alkhazov³⁷, P. Alvarez Cartelle⁴⁷, S. Amato², Y. Amhis¹¹, L. An²¹, L. Anderlini²¹, A. Andreianov³⁷, M. Andreotti²⁰, F. Archilli¹⁶, A. Artamonov⁴³, M. Artuso⁶⁷, K. Arzymatov⁴¹, E. Aslanides¹⁰, M. Atzeni⁴⁹, B. Audurier¹¹, S. Bachmann¹⁶, M. Bachmayer⁴⁸, J.J. Back⁵⁵, S. Baker⁶⁰, P. Baladron Rodriguez⁴⁵, V. Balagura¹¹, W. Baldini²⁰, J. Baptista Leite¹, R.J. Barlow⁶¹, S. Barsuk¹¹, W. Barter⁶⁰, M. Bartolini^{23,i}, F. Baryshnikov⁸⁰, J.M. Basels¹³, G. Bassi²⁸, B. Batsukh⁶⁷, A. Battig¹⁴, A. Bay⁴⁸, M. Becker¹⁴, F. Bedeschi²⁸, I. Bediaga¹, A. Beiter⁶⁷, V. Belavin⁴¹, S. Belin²⁶, V. Bellee⁴⁸, K. Belous⁴³, I. Belov³⁹, I. Belyaev³⁸, G. Bencivenni²², E. Ben-Haim¹², A. Berezhnoy³⁹, R. Bernet⁴⁹, D. Berninghoff¹⁶, H.C. Bernstein⁶⁷, C. Bertella⁴⁷, E. Bertholet¹², A. Bertolin²⁷, C. Betancourt⁴⁹, F. Betti^{19,e}, M.O. Bettler⁵⁴, Ia. Bezshyiko⁴⁹, S. Bhasin⁵³, J. Bhom³³, L. Bian⁷², M.S. Bieker¹⁴, S. Bifani⁵², P. Billoir¹², M. Birch⁶⁰, F.C.R. Bishop⁵⁴, A. Bizzeti^{21,s}, M. Bjørn⁶², M.P. Blago⁴⁷, T. Blake⁵⁵, F. Blanc⁴⁸, S. Blusk⁶⁷, D. Bobulska⁵⁸, V. Bocci³⁰, J.A. Boelhave¹⁴, O. Boente Garcia⁴⁵, T. Boettcher⁶³, A. Boldyrev⁸¹, A. Bondar^{42,v}, N. Bondar³⁷, S. Borghi⁶¹, M. Borisyak⁴¹, M. Borsato¹⁶, J.T. Borsuk³³, S.A. Bouchiba⁴⁸, T.J.V. Bowcock⁵⁹, A. Boyer⁴⁷, C. Bozzi²⁰, M.J. Bradley⁶⁰, S. Braun⁶⁵, A. Brea Rodriguez⁴⁵, M. Brodski⁴⁷, J. Brodzicka³³, A. Brossa Gonzalo⁵⁵, D. Brundu²⁶, A. Buonauro⁴⁹, C. Burr⁴⁷, A. Bursche²⁶, A. Butkevich⁴⁰, J.S. Butter³¹, J. Buytaert⁴⁷, W. Byczynski⁴⁷, S. Cadeddu²⁶, H. Cai⁷², R. Calabrese^{20,g}, L. Calefice¹⁴, L. Calero Diaz²², S. Cali²², R. Calladine⁵², M. Calvi^{24,j}, M. Calvo Gomez⁸³, P. Camargo Magalhaes⁵³, A. Camboni⁴⁴, P. Campana²², D.H. Campora Perez⁴⁷, A.F. Campoverde Quezada⁵, S. Capelli^{24,j}, L. Capriotti^{19,e}, A. Carbone^{19,e}, G. Carboni²⁹, R. Cardinale^{23,i}, A. Cardini²⁶, I. Carli⁶, P. Carniti^{24,j}, K. Carvalho Akiba³¹, A. Casais Vidal⁴⁵, G. Casse⁵⁹, M. Cattaneo⁴⁷, G. Cavallero⁴⁷, S. Celani⁴⁸, J. Cerasoli¹⁰, A.J. Chadwick⁵⁹, M.G. Chapman⁵³, M. Charles¹², Ph. Charpentier⁴⁷, G. Chatzikonstantinidis⁵², C.A. Chavez Barajas⁵⁹, M. Chefdeville⁸, C. Chen³, S. Chen²⁶, A. Chernov³³, S.-G. Chitic⁴⁷, V. Chobanova⁴⁵, S. Cholak⁴⁸, M. Chruszcz³³, A. Chubykin³⁷, V. Chulikov³⁷, P. Ciambrone²², M.F. Cicala⁵⁵, X. Cid Vidal⁴⁵, G. Ciezarek⁴⁷, P.E.L. Clarke⁵⁷, M. Clemencic⁴⁷, H.V. Cliff⁵⁴, J. Closier⁴⁷, J.L. Cobbledick⁶¹, V. Coco⁴⁷, J.A.B. Coelho¹¹, J. Cogan¹⁰, E. Cogneras⁹, L. Cojocariu³⁶, P. Collins⁴⁷, T. Colombo⁴⁷, L. Congedo¹⁸, A. Contu²⁶, N. Cooke⁵², G. Coombs⁵⁸, G. Corti⁴⁷, C.M. Costa Sobral⁵⁵, B. Couturier⁴⁷, D.C. Craik⁶³, J. Crkovská⁶⁶, M. Cruz Torres¹, R. Currie⁵⁷, C.L. Da Silva⁶⁶, E. Dall'Occo¹⁴, J. Dalseno⁴⁵, C. D'Ambrosio⁴⁷, A. Danilina³⁸, P. d'Argent⁴⁷, A. Davis⁶¹, O. De Aguiar Francisco⁶¹, K. De Bruyn⁷⁷, S. De Capua⁶¹, M. De Cian⁴⁸, J.M. De Miranda¹, L. De Paula², M. De Serio^{18,d}, D. De Simone⁴⁹, P. De Simone²², J.A. de Vries⁷⁸, C.T. Dean⁶⁶, W. Dean⁸⁴, D. Decamp⁸, L. Del Buono¹², B. Delaney⁵⁴, H.-P. Dembinski¹⁴, A. Dendek³⁴, V. Denysenko⁴⁹, D. Derkach⁸¹, O. Deschamps⁹, F. Desse¹¹, F. Dettori^{26,f}, B. Dey⁷², P. Di Nezza²², S. Didenko⁸⁰, L. Dieste Maronas⁴⁵, H. Dijkstra⁴⁷, V. Dobishuk⁵¹, A.M. Donohoe¹⁷, F. Dordei²⁶, M. Dorigo^{28,w}, A.C. dos Reis¹, L. Douglas⁵⁸, A. Dovbnya⁵⁰, A.G. Downes⁸, K. Dreimanis⁵⁹, M.W. Dudek³³, L. Dufour⁴⁷, V. Duk⁷⁶, P. Durante⁴⁷, J.M. Durham⁶⁶, D. Dutta⁶¹, M. Dziewiecki¹⁶, A. Dziurda³³, A. Dzyuba³⁷, S. Easo⁵⁶, U. Egede⁶⁸, V. Egorychev³⁸, S. Eidelman^{42,v}, S. Eisenhardt⁵⁷, S. Ek-In⁴⁸, L. Eklund⁵⁸, S. Ely⁶⁷, A. Ene³⁶, E. Eppele⁶⁶, S. Escher¹³, J. Eschle⁴⁹, S. Esen³¹, T. Evans⁴⁷, A. Falabella¹⁹, J. Fan³, Y. Fan⁵, B. Fang⁷², N. Farley⁵², S. Farry⁵⁹, D. Fazzini^{24,j}, P. Fedin³⁸, M. Féo⁴⁷, P. Fernandez Declara⁴⁷, A. Fernandez Prieto⁴⁵, J.M. Fernandez-tenllado Arribas⁴⁴, F. Ferrari^{19,e}, L. Ferreira Lopes⁴⁸, F. Ferreira Rodrigues², S. Ferreres Sole³¹, M. Ferrillo⁴⁹, M. Ferro-Luzzi⁴⁷, S. Filippov⁴⁰, R.A. Fini¹⁸, M. Fiorini^{20,g}, M. Firlej³⁴, K.M. Fischer⁶², C. Fitzpatrick⁶¹,

T. Fiutowski³⁴, F. Fleuret^{11,b}, M. Fontana⁴⁷, F. Fontanelli^{23,i}, R. Forty⁴⁷, V. Franco Lima⁵⁹, M. Franco Sevilla⁶⁵, M. Frank⁴⁷, E. Franzoso²⁰, G. Frau¹⁶, C. Frei⁴⁷, D.A. Friday⁵⁸, J. Fu²⁵, Q. Fuehring¹⁴, W. Funk⁴⁷, E. Gabriel³¹, T. Gaintseva⁴¹, A. Gallas Torreira⁴⁵, D. Galli^{19,e}, S. Gallorini²⁷, S. Gambetta⁵⁷, Y. Gan³, M. Gandelman², P. Gandini²⁵, Y. Gao⁴, M. Garau²⁶, L.M. Garcia Martin⁵⁵, P. Garcia Moreno⁴⁴, J. García Pardiñas⁴⁹, B. Garcia Plana⁴⁵, F.A. Garcia Rosales¹¹, L. Garrido⁴⁴, D. Gascon⁴⁴, C. Gaspar⁴⁷, R.E. Geertsema³¹, D. Gerick¹⁶, L.L. Gerken¹⁴, E. Gersabeck⁶¹, M. Gersabeck⁶¹, T. Gershon⁵⁵, D. Gerstel¹⁰, Ph. Ghez⁸, V. Gibson⁵⁴, M. Giovannetti^{22,k}, A. Gioventù⁴⁵, P. Gironella Gironell⁴⁴, L. Giubega³⁶, C. Giugliano^{20,g}, K. Gizdov⁵⁷, E.L. Gkougkousis⁴⁷, V.V. Gligorov¹², C. Göbel⁶⁹, E. Golobardes⁸³, D. Golubkov³⁸, A. Golutvin^{60,80}, A. Gomes^{1,a}, S. Gomez Fernandez⁴⁴, F. Goncalves Abrantes⁶⁹, M. Goncerz³³, G. Gong³, P. Gorbounov³⁸, I.V. Gorelov³⁹, C. Gotti^{24,j}, E. Govorkova³¹, J.P. Grabowski¹⁶, R. Graciani Diaz⁴⁴, T. Grammatico¹², L.A. Granado Cardoso⁴⁷, E. Graugés⁴⁴, E. Graverini⁴⁸, G. Graziani²¹, A. Grecu³⁶, L.M. Greeven³¹, P. Griffith²⁰, L. Grillo⁶¹, S. Gromov⁸⁰, L. Gruber⁴⁷, B.R. Gruberg Cazon⁶², C. Gu³, M. Guarise²⁰, P. A. Günther¹⁶, E. Gushchin⁴⁰, A. Guth¹³, Y. Guz^{43,47}, T. Gys⁴⁷, T. Hadavizadeh⁶⁸, G. Haefeli⁴⁸, C. Haen⁴⁷, J. Haimberger⁴⁷, S.C. Haines⁵⁴, T. Halewood-leagas⁵⁹, P.M. Hamilton⁶⁵, Q. Han⁷, X. Han¹⁶, T.H. Hancock⁶², S. Hansmann-Menzemer¹⁶, N. Harnew⁶², T. Harrison⁵⁹, C. Hasse⁴⁷, M. Hatch⁴⁷, J. He⁵, M. Hecker⁶⁰, K. Heijhoff³¹, K. Heinicke¹⁴, A.M. Hennequin⁴⁷, K. Hennessy⁵⁹, L. Henry^{25,46}, J. Heuel¹³, A. Hicheur², D. Hill⁶², M. Hilton⁶¹, S.E. Hollitt¹⁴, P.H. Hopchev⁴⁸, J. Hu¹⁶, J. Hu⁷¹, W. Hu⁷, W. Huang⁵, X. Huang⁷², W. Hulsbergen³¹, R.J. Hunter⁵⁵, M. Hushchyn⁸¹, D. Hutchcroft⁵⁹, D. Hynds³¹, P. Ibis¹⁴, M. Idzik³⁴, D. Ilin³⁷, P. Ilten⁵², A. Inglessi³⁷, A. Ishteev⁸⁰, K. Ivshin³⁷, R. Jacobsson⁴⁷, S. Jakobsen⁴⁷, E. Jans³¹, B.K. Jashal⁴⁶, A. Jawahery⁶⁵, V. Jevtic¹⁴, M. Jezabek³³, F. Jiang³, M. John⁶², D. Johnson⁴⁷, C.R. Jones⁵⁴, T.P. Jones⁵⁵, B. Jost⁴⁷, N. Jurik⁴⁷, S. Kandybei⁵⁰, Y. Kang³, M. Karacson⁴⁷, J.M. Kariuki⁵³, N. Kazeev⁸¹, M. Kecke¹⁶, F. Keizer^{54,47}, M. Kenzie⁵⁵, T. Ketel³², B. Khanji⁴⁷, A. Kharisova⁸², S. Kholodenko⁴³, K.E. Kim⁶⁷, T. Kirn¹³, V.S. Kirsebom⁴⁸, O. Kitouni⁶³, S. Klaver³¹, K. Klimaszewski³⁵, S. Koliiev⁵¹, A. Kondybayeva⁸⁰, A. Konoplyannikov³⁸, P. Kopciwicz³⁴, R. Kopečna¹⁶, P. Koppenburg³¹, M. Korolev³⁹, I. Kostiuik^{31,51}, O. Kot⁵¹, S. Kotriakhova^{37,30}, P. Kravchenko³⁷, L. Kravchuk⁴⁰, R.D. Krawczyk⁴⁷, M. Kreps⁵⁵, F. Kress⁶⁰, S. Kretzschmar¹³, P. Krokovny^{42,v}, W. Krupa³⁴, W. Krzemien³⁵, W. Kucewicz^{33,l}, M. Kucharczyk³³, V. Kudryavtsev^{42,v}, H.S. Kuindersma³¹, G.J. Kunde⁶⁶, T. Kvaratskheliya³⁸, D. Lacarrere⁴⁷, G. Lafferty⁶¹, A. Lai²⁶, A. Lampis²⁶, D. Lancierini⁴⁹, J.J. Lane⁶¹, R. Lane⁵³, G. Lanfranchi²², C. Langenbruch¹³, J. Langer¹⁴, O. Lantwin^{49,80}, T. Latham⁵⁵, F. Lazzari^{28,t}, R. Le Gac¹⁰, S.H. Lee⁸⁴, R. Lefèvre⁹, A. Leflat³⁹, S. Legotin⁸⁰, O. Leroy¹⁰, T. Lesiak³³, B. Leverington¹⁶, H. Li⁷¹, L. Li⁶², P. Li¹⁶, X. Li⁶⁶, Y. Li⁶, Y. Li⁶, Z. Li⁶⁷, X. Liang⁶⁷, T. Lin⁶⁰, R. Lindner⁴⁷, V. Lisovskyi¹⁴, R. Litvinov²⁶, G. Liu⁷¹, H. Liu⁵, S. Liu⁶, X. Liu³, A. Loi²⁶, J. Lomba Castro⁴⁵, I. Longstaff⁵⁸, J.H. Lopes², G. Loustau⁴⁹, G.H. Lovell⁵⁴, Y. Lu⁶, D. Lucchesi^{27,m}, S. Luchuk⁴⁰, M. Lucio Martinez³¹, V. Lukashenko³¹, Y. Luo³, A. Lupato⁶¹, E. Luppi^{20,g}, O. Lupton⁵⁵, A. Lusiani^{28,r}, X. Lyu⁵, L. Ma⁶, S. Maccolini^{19,e}, F. Machefert¹¹, F. Maciuc³⁶, V. Macko⁴⁸, P. Mackowiak¹⁴, S. Maddrell-Mander⁵³, O. Madejczyk³⁴, L.R. Madhan Mohan⁵³, O. Maev³⁷, A. Maevskiy⁸¹, D. Maisuzenko³⁷, M.W. Majewski³⁴, S. Malde⁶², B. Malecki⁴⁷, A. Malinin⁷⁹, T. Maltsev^{42,v}, H. Malygina¹⁶, G. Manca^{26,f}, G. Mancinelli¹⁰, R. Manera Escalero⁴⁴, D. Manuzzi^{19,e}, D. Marangotto^{25,o}, J. Maratas^{9,u}, J.F. Marchand⁸, U. Marconi¹⁹, S. Mariani^{21,47,h}, C. Marin Benito¹¹, M. Marinangeli⁴⁸, P. Marino⁴⁸, J. Marks¹⁶, P.J. Marshall⁵⁹, G. Martellotti³⁰, L. Martinazzoli^{47,j}, M. Martinelli^{24,j}, D. Martinez Santos⁴⁵, F. Martinez Vidal⁴⁶, A. Massafferri¹, M. Materok¹³, R. Matev⁴⁷, A. Mathad⁴⁹, Z. Mathe⁴⁷, V. Matiunin³⁸, C. Matteuzzi²⁴, K.R. Mattioli⁸⁴, A. Mauri³¹, E. Maurice^{11,b}, J. Mauricio⁴⁴, M. Mazurek³⁵, M. McCann⁶⁰, L. McConnell¹⁷, T.H. McGrath⁶¹, A. McNab⁶¹, R. McNulty¹⁷, J.V. Mead⁵⁹, B. Meadows⁶⁴,

C. Meaux¹⁰, G. Meier¹⁴, N. Meinert⁷⁵, D. Melnychuk³⁵, S. Meloni^{24,j}, M. Merk^{31,78}, A. Merli²⁵, L. Meyer Garcia², M. Mikhasenko⁴⁷, D.A. Milanese⁷³, E. Millard⁵⁵, M. Milovanovic⁴⁷, M.-N. Minard⁸, L. Minzoni^{20,g}, S.E. Mitchell⁵⁷, B. Mitreska⁶¹, D.S. Mitzel⁴⁷, A. Mödden¹⁴, R.A. Mohammed⁶², R.D. Moise⁶⁰, T. Mombächer¹⁴, I.A. Monroy⁷³, S. Monteil⁹, M. Morandin²⁷, G. Morello²², M.J. Morello^{28,r}, J. Moron³⁴, A.B. Morris⁷⁴, A.G. Morris⁵⁵, R. Mountain⁶⁷, H. Mu³, F. Muheim⁵⁷, M. Mukherjee⁷, M. Mulder⁴⁷, D. Müller⁴⁷, K. Müller⁴⁹, C.H. Murphy⁶², D. Murray⁶¹, P. Muzzetto²⁶, P. Naik⁵³, T. Nakada⁴⁸, R. Nandakumar⁵⁶, T. Nanut⁴⁸, I. Nasteva², M. Needham⁵⁷, I. Neri^{20,g}, N. Neri^{25,o}, S. Neubert⁷⁴, N. Neufeld⁴⁷, R. Newcombe⁶⁰, T.D. Nguyen⁴⁸, C. Nguyen-Mau⁴⁸, E.M. Niel¹¹, S. Nieswand¹³, N. Nikitin³⁹, N.S. Nolte⁴⁷, C. Nunez⁸⁴, A. Oblakowska-Mucha³⁴, V. Obraztsov⁴³, D.P. O’Hanlon⁵³, R. Oldeman^{26,f}, C.J.G. Onderwater⁷⁷, A. Ossowska³³, J.M. Otalora Goicochea², T. Ovsiannikova³⁸, P. Owen⁴⁹, A. Oyanguren⁴⁶, B. Pagare⁵⁵, P.R. Pais⁴⁷, T. Pajero^{28,47,r}, A. Palano¹⁸, M. Palutan²², Y. Pan⁶¹, G. Panshin⁸², A. Papanestis⁵⁶, M. Pappagallo^{18,d}, L.L. Pappalardo^{20,g}, C. Pappenheimer⁶⁴, W. Parker⁶⁵, C. Parkes⁶¹, C.J. Parkinson⁴⁵, B. Passalacqua²⁰, G. Passaleva²¹, A. Pastore¹⁸, M. Patel⁶⁰, C. Patrignani^{19,e}, C.J. Pawley⁷⁸, A. Pearce⁴⁷, A. Pellegrino³¹, M. Pepe Altarelli⁴⁷, S. Perazzini¹⁹, D. Pereima³⁸, P. Perret⁹, K. Petridis⁵³, A. Petrolini^{23,i}, A. Petrov⁷⁹, S. Petrucci⁵⁷, M. Petruzzo²⁵, A. Philippov⁴¹, L. Pica²⁸, M. Piccini⁷⁶, B. Pietrzyk⁸, G. Pietrzyk⁴⁸, M. Pili⁶², D. Pinci³⁰, J. Pinzino⁴⁷, F. Pisani⁴⁷, A. Piucci¹⁶, Resmi P.K¹⁰, V. Placinta³⁶, S. Playfer⁵⁷, J. Plews⁵², M. Plo Casasus⁴⁵, F. Polci¹², M. Poli Lener²², M. Poliakova⁶⁷, A. Poluektov¹⁰, N. Polukhina^{80,c}, I. Polyakov⁶⁷, E. Polycarpo², G.J. Pomery⁵³, S. Ponce⁴⁷, A. Popov⁴³, D. Popov^{5,47}, S. Popov⁴¹, S. Poslavskii⁴³, K. Prasanth³³, L. Promberger⁴⁷, C. Prouve⁴⁵, V. Pugatch⁵¹, A. Puig Navarro⁴⁹, H. Pullen⁶², G. Punzi^{28,n}, W. Qian⁵, J. Qin⁵, R. Quagliani¹², B. Quintana⁸, N.V. Raab¹⁷, R.I. Rabadan Trejo¹⁰, B. Rachwal³⁴, J.H. Rademacker⁵³, M. Rama²⁸, M. Ramos Pernas⁵⁵, M.S. Rangel², F. Ratnikov^{41,81}, G. Raven³², M. Reboud⁸, F. Redi⁴⁸, F. Reiss¹², C. Remon Alepuz⁴⁶, Z. Ren³, V. Renaudin⁶², R. Ribatti²⁸, S. Ricciardi⁵⁶, D.S. Richards⁵⁶, K. Rinnert⁵⁹, P. Robbe¹¹, A. Robert¹², G. Robertson⁵⁷, A.B. Rodrigues⁴⁸, E. Rodrigues⁵⁹, J.A. Rodriguez Lopez⁷³, A. Rollings⁶², P. Roloff⁴⁷, V. Romanovskiy⁴³, M. Romero Lamas⁴⁵, A. Romero Vidal⁴⁵, J.D. Roth⁸⁴, M. Rotondo²², M.S. Rudolph⁶⁷, T. Ruf⁴⁷, J. Ruiz Vidal⁴⁶, A. Ryzhikov⁸¹, J. Ryzka³⁴, J.J. Saborido Silva⁴⁵, N. Sagidova³⁷, N. Sahoo⁵⁵, B. Saitta^{26,f}, D. Sanchez Gonzalo⁴⁴, C. Sanchez Gras³¹, C. Sanchez Mayordomo⁴⁶, R. Santacesaria³⁰, C. Santamarina Rios⁴⁵, M. Santimaria²², E. Santovetti^{29,k}, D. Saranin⁸⁰, G. Sarpis⁶¹, M. Sarpis⁷⁴, A. Sarti³⁰, C. Satriano^{30,q}, A. Satta²⁹, M. Saur⁵, D. Savrina^{38,39}, H. Sazak⁹, L.G. Scantlebury Smead⁶², S. Schael¹³, M. Schellenberg¹⁴, M. Schiller⁵⁸, H. Schindler⁴⁷, M. Schmelling¹⁵, T. Schmelzer¹⁴, B. Schmidt⁴⁷, O. Schneider⁴⁸, A. Schopper⁴⁷, M. Schubiger³¹, S. Schulte⁴⁸, M.H. Schune¹¹, R. Schwemmer⁴⁷, B. Sciascia²², A. Sciubba³⁰, S. Sellam⁴⁵, A. Semennikov³⁸, M. Senghi Soares³², A. Sergi^{52,47}, N. Serra⁴⁹, J. Serrano¹⁰, L. Sestini²⁷, A. Seuthe¹⁴, P. Seyfert⁴⁷, D.M. Shangase⁸⁴, M. Shapkin⁴³, I. Shchemerov⁸⁰, L. Shchutska⁴⁸, T. Shears⁵⁹, L. Shekhtman^{42,v}, Z. Shen⁴, V. Shevchenko⁷⁹, E.B. Shields^{24,j}, E. Shmanin⁸⁰, J.D. Shupperd⁶⁷, B.G. Siddi²⁰, R. Silva Coutinho⁴⁹, G. Simi²⁷, S. Simone^{18,d}, I. Skiba^{20,g}, N. Skidmore⁷⁴, T. Skwarnicki⁶⁷, M.W. Slater⁵², J.C. Smallwood⁶², J.G. Smeaton⁵⁴, A. Smetkina³⁸, E. Smith¹³, M. Smith⁶⁰, A. Snoch³¹, M. Soares¹⁹, L. Soares Lavra⁹, M.D. Sokoloff⁶⁴, F.J.P. Soler⁵⁸, A. Solovev³⁷, I. Solovye³⁷, F.L. Souza De Almeida², B. Souza De Paula², B. Spaan¹⁴, E. Spadaro Norella^{25,o}, P. Spradlin⁵⁸, F. Stagni⁴⁷, M. Stahl⁶⁴, S. Stahl⁴⁷, P. Steffen⁴⁸, O. Steinkamp^{49,80}, S. Stemmler¹⁶, O. Stenyakin⁴³, H. Stevens¹⁴, S. Stone⁶⁷, M.E. Stramaglia⁴⁸, M. Straticiu³⁶, D. Strelakina⁸⁰, S. Strokov⁸², F. Suljik⁶², J. Sun²⁶, L. Sun⁷², Y. Sun⁶⁵, P. Svihra⁶¹, P.N. Swallow⁵², K. Swientek³⁴, A. Szabelski³⁵, T. Szumlak³⁴, M. Szymanski⁴⁷, S. Taneja⁶¹, Z. Tang³, T. Tekampe¹⁴, F. Teubert⁴⁷, E. Thomas⁴⁷, K.A. Thomson⁵⁹, M.J. Tilley⁶⁰, V. Tisserand⁹, S. T’Jampens⁸, M. Tobin⁶, S. Tol⁴⁷,

L. Tomassetti^{20,g}, D. Torres Machado¹, D.Y. Tou¹², M. Traill⁵⁸, M.T. Tran⁴⁸, E. Trifonova⁸⁰, C. Tripl⁴⁸, A. Tsaregorodtsev¹⁰, G. Tuci^{28,n}, A. Tully⁴⁸, N. Tuning³¹, A. Ukleja³⁵, D.J. Unverzagt¹⁶, A. Usachov³¹, A. Ustyuzhanin^{41,81}, U. Uwer¹⁶, A. Vagner⁸², V. Vagnoni¹⁹, A. Valassi⁴⁷, G. Valenti¹⁹, N. Valls Canudas⁴⁴, M. van Beuzekom³¹, H. Van Hecke⁶⁶, E. van Herwijnen⁸⁰, C.B. Van Hulse¹⁷, M. van Veghel⁷⁷, R. Vazquez Gomez⁴⁵, P. Vazquez Regueiro⁴⁵, C. Vázquez Sierra³¹, S. Vecchi²⁰, J.J. Velthuis⁵³, M. Veltri^{21,p}, A. Venkateswaran⁶⁷, M. Veronesi³¹, M. Vesterinen⁵⁵, D. Vieira⁶⁴, M. Vieites Diaz⁴⁸, H. Viemann⁷⁵, X. Vilasis-Cardona⁸³, E. Vilella Figueras⁵⁹, P. Vincent¹², G. Vitali²⁸, A. Vollhardt⁴⁹, D. Vom Bruch¹², A. Vorobyev³⁷, V. Vorobyev^{42,v}, N. Voropaev³⁷, R. Waldi⁷⁵, J. Walsh²⁸, C. Wang¹⁶, J. Wang³, J. Wang⁷², J. Wang⁴, J. Wang⁶, M. Wang³, R. Wang⁵³, Y. Wang⁷, Z. Wang⁴⁹, D.R. Ward⁵⁴, H.M. Wark⁵⁹, N.K. Watson⁵², S.G. Weber¹², D. Websdale⁶⁰, C. Weisser⁶³, B.D.C. Westhenry⁵³, D.J. White⁶¹, M. Whitehead⁵³, D. Wiedner¹⁴, G. Wilkinson⁶², M. Wilkinson⁶⁷, I. Williams⁵⁴, M. Williams^{63,68}, M.R.J. Williams⁵⁷, F.F. Wilson⁵⁶, W. Wislicki³⁵, M. Witek³³, L. Witola¹⁶, G. Wormser¹¹, S.A. Wotton⁵⁴, H. Wu⁶⁷, K. Wyllie⁴⁷, Z. Xiang⁵, D. Xiao⁷, Y. Xie⁷, H. Xing⁷¹, A. Xu⁴, J. Xu⁵, L. Xu³, M. Xu⁷, Q. Xu⁵, Z. Xu⁵, Z. Xu⁴, D. Yang³, Y. Yang⁵, Z. Yang³, Z. Yang⁶⁵, Y. Yao⁶⁷, L.E. Yeomans⁵⁹, H. Yin⁷, J. Yu⁷⁰, X. Yuan⁶⁷, O. Yushchenko⁴³, K.A. Zarebski⁵², M. Zavertyaev^{15,c}, M. Zdybal³³, O. Zenaiev⁴⁷, M. Zeng³, D. Zhang⁷, L. Zhang³, S. Zhang⁴, Y. Zhang⁴⁷, Y. Zhang⁶², A. Zhelezov¹⁶, Y. Zheng⁵, X. Zhou⁵, Y. Zhou⁵, X. Zhu³, V. Zhukov^{13,39}, J.B. Zonneveld⁵⁷, S. Zucchelli^{19,e}, D. Zuliani²⁷ and G. Zunica⁶¹

¹ *Centro Brasileiro de Pesquisas Físicas (CBPF), Rio de Janeiro, Brazil*

² *Universidade Federal do Rio de Janeiro (UFRJ), Rio de Janeiro, Brazil*

³ *Center for High Energy Physics, Tsinghua University, Beijing, China*

⁴ *School of Physics State Key Laboratory of Nuclear Physics and Technology, Peking University, Beijing, China*

⁵ *University of Chinese Academy of Sciences, Beijing, China*

⁶ *Institute Of High Energy Physics (IHEP), Beijing, China*

⁷ *Institute of Particle Physics, Central China Normal University, Wuhan, Hubei, China*

⁸ *Univ. Grenoble Alpes, Univ. Savoie Mont Blanc, CNRS, IN2P3-LAPP, Annecy, France*

⁹ *Université Clermont Auvergne, CNRS/IN2P3, LPC, Clermont-Ferrand, France*

¹⁰ *Aix Marseille Univ, CNRS/IN2P3, CPPM, Marseille, France*

¹¹ *Ijclab, Orsay, France*

¹² *LPNHE, Sorbonne Université, Paris Diderot Sorbonne Paris Cité, CNRS/IN2P3, Paris, France*

¹³ *I. Physikalisches Institut, RWTH Aachen University, Aachen, Germany*

¹⁴ *Fakultät Physik, Technische Universität Dortmund, Dortmund, Germany*

¹⁵ *Max-Planck-Institut für Kernphysik (MPIK), Heidelberg, Germany*

¹⁶ *Physikalisches Institut, Ruprecht-Karls-Universität Heidelberg, Heidelberg, Germany*

¹⁷ *School of Physics, University College Dublin, Dublin, Ireland*

¹⁸ *INFN Sezione di Bari, Bari, Italy*

¹⁹ *INFN Sezione di Bologna, Bologna, Italy*

²⁰ *INFN Sezione di Ferrara, Ferrara, Italy*

²¹ *INFN Sezione di Firenze, Firenze, Italy*

²² *INFN Laboratori Nazionali di Frascati, Frascati, Italy*

²³ *INFN Sezione di Genova, Genova, Italy*

²⁴ *INFN Sezione di Milano-Bicocca, Milano, Italy*

²⁵ *INFN Sezione di Milano, Milano, Italy*

²⁶ *INFN Sezione di Cagliari, Monserrato, Italy*

²⁷ *Università degli Studi di Padova, Università e INFN, Padova, Padova, Italy*

²⁸ *INFN Sezione di Pisa, Pisa, Italy*

²⁹ *INFN Sezione di Roma Tor Vergata, Roma, Italy*

- ³⁰ INFN Sezione di Roma La Sapienza, Roma, Italy
- ³¹ Nikhef National Institute for Subatomic Physics, Amsterdam, Netherlands
- ³² Nikhef National Institute for Subatomic Physics and VU University Amsterdam, Amsterdam, Netherlands
- ³³ Henryk Niewodniczanski Institute of Nuclear Physics Polish Academy of Sciences, Kraków, Poland
- ³⁴ AGH - University of Science and Technology, Faculty of Physics and Applied Computer Science, Kraków, Poland
- ³⁵ National Center for Nuclear Research (NCBJ), Warsaw, Poland
- ³⁶ Horia Hulubei National Institute of Physics and Nuclear Engineering, Bucharest-Magurele, Romania
- ³⁷ Petersburg Nuclear Physics Institute NRC Kurchatov Institute (PNPI NRC KI), Gatchina, Russia
- ³⁸ Institute of Theoretical and Experimental Physics NRC Kurchatov Institute (ITEP NRC KI), Moscow, Russia
- ³⁹ Institute of Nuclear Physics, Moscow State University (SINP MSU), Moscow, Russia
- ⁴⁰ Institute for Nuclear Research of the Russian Academy of Sciences (INR RAS), Moscow, Russia
- ⁴¹ Yandex School of Data Analysis, Moscow, Russia
- ⁴² Budker Institute of Nuclear Physics (SB RAS), Novosibirsk, Russia
- ⁴³ Institute for High Energy Physics NRC Kurchatov Institute (IHEP NRC KI), Protvino, Russia, Protvino, Russia
- ⁴⁴ ICCUB, Universitat de Barcelona, Barcelona, Spain
- ⁴⁵ Instituto Galego de Física de Altas Enerxías (IGFAE), Universidade de Santiago de Compostela, Santiago de Compostela, Spain
- ⁴⁶ Instituto de Física Corpuscular, Centro Mixto Universidad de Valencia - CSIC, Valencia, Spain
- ⁴⁷ European Organization for Nuclear Research (CERN), Geneva, Switzerland
- ⁴⁸ Institute of Physics, Ecole Polytechnique Fédérale de Lausanne (EPFL), Lausanne, Switzerland
- ⁴⁹ Physik-Institut, Universität Zürich, Zürich, Switzerland
- ⁵⁰ NSC Kharkiv Institute of Physics and Technology (NSC KIPT), Kharkiv, Ukraine
- ⁵¹ Institute for Nuclear Research of the National Academy of Sciences (KINR), Kyiv, Ukraine
- ⁵² University of Birmingham, Birmingham, United Kingdom
- ⁵³ H.H. Wills Physics Laboratory, University of Bristol, Bristol, United Kingdom
- ⁵⁴ Cavendish Laboratory, University of Cambridge, Cambridge, United Kingdom
- ⁵⁵ Department of Physics, University of Warwick, Coventry, United Kingdom
- ⁵⁶ STFC Rutherford Appleton Laboratory, Didcot, United Kingdom
- ⁵⁷ School of Physics and Astronomy, University of Edinburgh, Edinburgh, United Kingdom
- ⁵⁸ School of Physics and Astronomy, University of Glasgow, Glasgow, United Kingdom
- ⁵⁹ Oliver Lodge Laboratory, University of Liverpool, Liverpool, United Kingdom
- ⁶⁰ Imperial College London, London, United Kingdom
- ⁶¹ Department of Physics and Astronomy, University of Manchester, Manchester, United Kingdom
- ⁶² Department of Physics, University of Oxford, Oxford, United Kingdom
- ⁶³ Massachusetts Institute of Technology, Cambridge, MA, United States
- ⁶⁴ University of Cincinnati, Cincinnati, OH, United States
- ⁶⁵ University of Maryland, College Park, MD, United States
- ⁶⁶ Los Alamos National Laboratory (LANL), Los Alamos, United States
- ⁶⁷ Syracuse University, Syracuse, NY, United States
- ⁶⁸ School of Physics and Astronomy, Monash University, Melbourne, Australia, associated to ⁵⁵
- ⁶⁹ Pontifícia Universidade Católica do Rio de Janeiro (PUC-Rio), Rio de Janeiro, Brazil, associated to ²
- ⁷⁰ Physics and Micro Electronic College, Hunan University, Changsha City, China, associated to ⁷
- ⁷¹ Guangdong Provincial Key Laboratory of Nuclear Science, Institute of Quantum Matter, South China Normal University, Guangzhou, China, associated to ³
- ⁷² School of Physics and Technology, Wuhan University, Wuhan, China, associated to ³
- ⁷³ Departamento de Física, Universidad Nacional de Colombia, Bogota, Colombia, associated to ¹²

- ⁷⁴ *Universität Bonn - Helmholtz-Institut für Strahlen und Kernphysik, Bonn, Germany, associated to* ¹⁶
- ⁷⁵ *Institut für Physik, Universität Rostock, Rostock, Germany, associated to* ¹⁶
- ⁷⁶ *INFN Sezione di Perugia, Perugia, Italy, associated to* ²⁰
- ⁷⁷ *Van Swinderen Institute, University of Groningen, Groningen, Netherlands, associated to* ³¹
- ⁷⁸ *Universiteit Maastricht, Maastricht, Netherlands, associated to* ³¹
- ⁷⁹ *National Research Centre Kurchatov Institute, Moscow, Russia, associated to* ³⁸
- ⁸⁰ *National University of Science and Technology “MISIS”, Moscow, Russia, associated to* ³⁸
- ⁸¹ *National Research University Higher School of Economics, Moscow, Russia, associated to* ⁴¹
- ⁸² *National Research Tomsk Polytechnic University, Tomsk, Russia, associated to* ³⁸
- ⁸³ *DS4DS, La Salle, Universitat Ramon Llull, Barcelona, Spain, associated to* ⁴⁴
- ⁸⁴ *University of Michigan, Ann Arbor, United States, associated to* ⁶⁷
- ^a *Universidade Federal do Triângulo Mineiro (UFTM), Uberaba-MG, Brazil*
- ^b *Laboratoire Leprince-Ringuet, Palaiseau, France*
- ^c *P.N. Lebedev Physical Institute, Russian Academy of Science (LPI RAS), Moscow, Russia*
- ^d *Università di Bari, Bari, Italy*
- ^e *Università di Bologna, Bologna, Italy*
- ^f *Università di Cagliari, Cagliari, Italy*
- ^g *Università di Ferrara, Ferrara, Italy*
- ^h *Università di Firenze, Firenze, Italy*
- ⁱ *Università di Genova, Genova, Italy*
- ^j *Università di Milano Bicocca, Milano, Italy*
- ^k *Università di Roma Tor Vergata, Roma, Italy*
- ^l *AGH - University of Science and Technology, Faculty of Computer Science, Electronics and Telecommunications, Kraków, Poland*
- ^m *Università di Padova, Padova, Italy*
- ⁿ *Università di Pisa, Pisa, Italy*
- ^o *Università degli Studi di Milano, Milano, Italy*
- ^p *Università di Urbino, Urbino, Italy*
- ^q *Università della Basilicata, Potenza, Italy*
- ^r *Scuola Normale Superiore, Pisa, Italy*
- ^s *Università di Modena e Reggio Emilia, Modena, Italy*
- ^t *Università di Siena, Siena, Italy*
- ^u *MSU - Iligan Institute of Technology (MSU-IIT), Iligan, Philippines*
- ^v *Novosibirsk State University, Novosibirsk, Russia*
- ^w *INFN Sezione di Trieste, Trieste, Italy*